The Plant Cell, Vol. 20: 1040–1058, April 2008, www.plantcell.org © 2008 American Society of Plant Biologists

β-AMYLASE4, a Noncatalytic Protein Required for Starch Breakdown, Acts Upstream of Three Active β-Amylases in *Arabidopsis* Chloroplasts [W] [OA]

Daniel C. Fulton,[a,1] Michaela Stettler,[b,1] Tabea Mettler,[b] Cara K. Vaughan,[c] Jing Li,[d] Perigio Francisco,[d] Manuel Gil,[e] Heike Reinhold,[b] Simona Eicke,[b] Gaëlle Messerli,[b] Gary Dorken,[a] Karen Halliday,[a] Alison M. Smith,[f] Steven M. Smith,[d] and Samuel C. Zeeman[b,2]

[a] Institute of Molecular Plant Sciences, University of Edinburgh, Edinburgh EH9 3JH, United Kingdom
[b] Institute of Plant Sciences, ETH Zurich, CH-8092 Zurich, Switzerland
[c] School of Crystallography, Birkbeck College, University of London, London WC1E 7HX, United Kingdom
[d] Centre of Excellence for Plant Metabolomics and Australian Research Council Centre of Excellence in Plant Energy Biology, University of Western Australia, Crawley WA 6009, Australia
[e] Institute for Computational Science, ETH Zurich, CH-8092 Zurich, Switzerland
[f] John Innes Centre, Norwich NR4 7UH, United Kingdom

This work investigated the roles of β-amylases in the breakdown of leaf starch. Of the nine β-amylase (BAM)–like proteins encoded in the *Arabidopsis thaliana* genome, at least four (BAM1, -2, -3, and -4) are chloroplastic. When expressed as recombinant proteins in *Escherichia coli*, BAM1, BAM2, and BAM3 had measurable β-amylase activity but BAM4 did not. BAM4 has multiple amino acid substitutions relative to characterized β-amylases, including one of the two catalytic residues. Modeling predicts major differences between the glucan binding site of BAM4 and those of active β-amylases. Thus, BAM4 probably lost its catalytic capacity during evolution. Total β-amylase activity was reduced in leaves of *bam1* and *bam3* mutants but not in *bam2* and *bam4* mutants. The *bam3* mutant had elevated starch levels and lower nighttime maltose levels than the wild type, whereas *bam1* did not. However, the *bam1 bam3* double mutant had a more severe phenotype than *bam3*, suggesting functional overlap between the two proteins. Surprisingly, *bam4* mutants had elevated starch levels. Introduction of the *bam4* mutation into the *bam3* and *bam1 bam3* backgrounds further elevated the starch levels in both cases. These data suggest that BAM4 facilitates or regulates starch breakdown and operates independently of BAM1 and BAM3. Together, our findings are consistent with the proposal that β-amylase is a major enzyme of starch breakdown in leaves, but they reveal unexpected complexity in terms of the specialization of protein function.

INTRODUCTION

Starch is a major product of photosynthesis in the leaves of many plants. It is synthesized in the chloroplast during the day from photoassimilated carbon and degraded throughout the following night to support metabolism (Zeeman et al., 2007). Recently, significant progress has been made in understanding the pathways of starch degradation in leaves. Several studies of *Arabidopsis thaliana* and other species indicate that maltose is the major product of starch hydrolysis and that it is exported from the chloroplast at night. First, the maltose content of leaves increases during the night when leaf starch is broken down (Niittylä et al., 2004; Weise et al., 2004). Second, the chloroplast envelope is permeable to maltose (Rost et al., 1996), and maltose is exported from intact, isolated chloroplasts that degrade starch (Weise et al., 2004). Loss of the chloroplast envelope maltose transporter MEX1 causes maltose to accumulate to very high levels in the chloroplast and retards starch breakdown (Niittylä et al., 2004; Lu et al., 2006). Third, loss of a maltose-metabolizing transglucosidase (DPE2) also causes maltose to accumulate to very high levels and retards starch breakdown in both *Arabidopsis* (Chia et al., 2004; Lu and Sharkey, 2004) and potato (*Solanum tuberosum*) (Lloyd et al., 2004). In *Arabidopsis*, DPE2 is located in the cytosol (Chia et al., 2004), and the maltose levels in *dpe2* mutants are elevated both inside and outside the chloroplast (Lu et al., 2006).

Although it is clear that maltose is the major product of starch degradation inside the chloroplast, the mechanism of its production from starch remains to be clarified. Two enzymes, α-amylase and β-amylase, could potentially produce maltose through the hydrolysis of amylopectin and amylose, the glucans that constitute starch. α-Amylase is an endohydrolase and can degrade glucans to yield a variety of linear and branched maltooligosaccharides, including α-maltose. However, it is unlikely that α-amylolysis is a major source of maltose during starch

[1] These authors contributed equally to this work.
[2] Address correspondence to szeeman@ethz.ch.
The author responsible for distribution of materials integral to the findings presented in this article in accordance with the policy described in the Instructions for Authors (www.plantcell.org) is: Samuel C. Zeeman (szeeman@ethz.ch).
[W] Online version contains Web-only data.
[OA] Open Access articles can be viewed online without a subscription.
www.plantcell.org/cgi/doi/10.1105/tpc.107.056507

breakdown. Mutation of all three α-amylase genes in *Arabidopsis* does not affect starch breakdown under normal growth room conditions (Yu et al., 2005). By contrast, β-amylase is an exohydrolase that acts at the nonreducing ends of α-1,4–linked glucan chains to produce β-maltose. Currently, experimental evidence favors β-amylolysis as the source of maltose during starch breakdown. Weise et al. (2005) showed that the maltose produced during starch breakdown is predominantly β-maltose. Furthermore, elevated levels of leaf starch were observed as a result of silencing of a gene encoding a chloroplast-targeted β-amylase in potato (Scheidig et al., 2002) and its ortholog in *Arabidopsis* (*BAM3*, also called CT-*BMY* and *BMY8*; for *Arabidopsis* gene information, including alternative nomenclature and references, see Supplemental Table 1 online).

Plant genomes encode multiple β-amylase–like proteins. In *Arabidopsis*, there are nine genes, which Smith et al. (2004) designated *BAM1* to *BAM9* to provide a unifying nomenclature. Of these nine, only *BAM3* has been implicated in starch degradation to date (Lao et al., 1999; Kaplan and Guy, 2005). Recently, Sparla et al. (2006) showed that *BAM1* (also called TR-*BMY* and *BMY7*), like *BAM3*, encodes an active, chloroplast-targeted β-amylase. Interestingly, BAM1 is regulated via thioredoxin-mediated reduction (hence the abbreviation TR-BMY; Sparla et al., 2006). However, initial reports suggest that mutation of *BAM1* does not result in excess leaf starch, and its function is not yet defined (Kaplan and Guy, 2005). BAM2 (also called BMY9) and BAM4 (also called BMY6) also have predicted N-terminal chloroplast transit peptides (Lloyd et al., 2005; Smith et al., 2005). However, the predictions are weak, and neither protein has been localized experimentally. In addition, Kaplan and Guy (2005) reported that mutation of *BAM2* did not result in elevated leaf starch.

Intriguingly, several of the β-amylase proteins are predicted to be localized outside the chloroplast, and their functions are unknown. Of these, only BAM5 (also called BMY1 and RAM1) has been studied in depth. Laby et al. (2001) reported that ~90% of the β-amylase activity in *Arabidopsis* leaves is encoded by the *BAM5* locus. Previously, it was reported that the BAM5 protein is localized to the phloem sieve elements (Wang et al., 1995). However, mutation of the *BAM5* gene does not appear to affect phloem function or leaf starch levels (Laby et al., 2001). To gain more insight into the roles of the β-amylases, we investigated the phylogeny of the β-amylase gene family and used reverse genetics to systematically study the functions of those proteins predicted to be targeted to the chloroplast. Our data strongly support the hypothesis that β-amylase is a major enzyme of starch breakdown but also indicate the specialization of BAM family members, including a novel role for a catalytically inactive, β-amylase–like protein in metabolic regulation.

RESULTS

Multiple Genes Encode β-Amylase in *Arabidopsis*

The nine genes encoding putative β-amylases in *Arabidopsis* (BAM1 to BAM9) are listed in Supplemental Table 1 online, along with Arabidopsis Genome Initiative numbers, references, alternative gene nomenclature, plus localization and transit peptide information. Using these proteins and β-amylases from other plant species, we performed a phylogenetic analysis of the conserved glucosyl hydrolase domain (~420 amino acid residues; see Supplemental Table 2 online). This analysis revealed four major subfamilies (Figure 1A). Subfamily I contains two *Arabidopsis* proteins, BAM5 and BAM6. This subfamily also includes the soybean (*Glycine max*) protein Gm BMY1 and the sweet potato (*Ipomoea batatas*) β-amylase Ib BMY1, the crystal structures of which have been solved (Mikami et al., 1993, 1994; Cheong et al., 1995). The genes upstream and downstream of the *BAM5* and *BAM6* genes in *Arabidopsis* are conserved, suggesting that these genes are paralogs resulting from a recent segmental duplication within the *Arabidopsis* genome. Subfamily I also contains monocot proteins, which group together on a subbranch separate from that of the dicot proteins. Subfamily II contains BAM1 and BAM3, the two proteins shown to encode active, chloroplastic enzymes (Lao et al., 1999; Sparla et al., 2006). Both *Arabidopsis* proteins have putative orthologs in other species, including rice (*Oryza sativa*) and poplar (*Populus* sp). Subfamily III contains monocot and dicot sequences including the *Arabidopsis* proteins BAM4 and BAM9. The sequences in this subfamily are more divergent than those in the other three. Finally, BAM2, -7, and -8 are contained in subfamily IV, together with an annotated rice protein and two annotated poplar proteins. The *BAM2* and *BAM7* genes are also putative paralogs, residing on recently duplicated segments of the genome.

We used the intron/exon structure to infer the evolutionary relationships between members of the *Arabidopsis BAM* gene family (Figure 1B). Consistent with the genome and phylogenetic analysis, *BAM5* and *BAM6* (subfamily I) have similar gene structures with seven exons in conserved positions. Similarly, *BAM1* and *BAM3* (subfamily II) genes are alike, with four exons. The core nine-exon structure of *BAM2*, *BAM7*, and *BAM8* (subfamily IV) are also similar, although these genes differ at the 5′ and 3′ ends. The structures of *BAM4* and *BAM9* (subfamily III) are dissimilar to each other and to the rest of the *BAM* genes.

Chloroplast Targeting

We analyzed the N-terminal regions of the encoded proteins for the presence of possible chloroplast transit peptides using ChloroP and TargetP, neural network–based methods for identifying targeting information in peptide sequences (Emanuelsson et al., 1999, 2000). BAM1 and BAM3 both possess predicted chloroplast transit peptides, consistent with their demonstrated chloroplastic locations (Lao et al., 1999; Sparla et al., 2006). BAM2 also has a predicted chloroplast transit peptide, but its duplicate, BAM7, does not. This can be explained by differences in the N termini of these two proteins. BAM7, like BAM8 and other members of subfamily IV, has an N-terminal extension of ~150 amino acids compared with BAM2. We hypothesize that BAM2 lost its N-terminal domain via a DNA insertion/deletion event, resulting in a cryptic transit peptide sequence. The chloroplast localization predictions are variable for BAM4 and BAM8. For both, ChloroP predicts that the protein is chloroplastic, whereas TargetP does not recognize any targeting information. Neither ChloroP nor TargetP predicts plastidial localization for BAM5, -6, -7, and -9. Thus, BAM1, -2, -3, -4, and -8 are the most likely

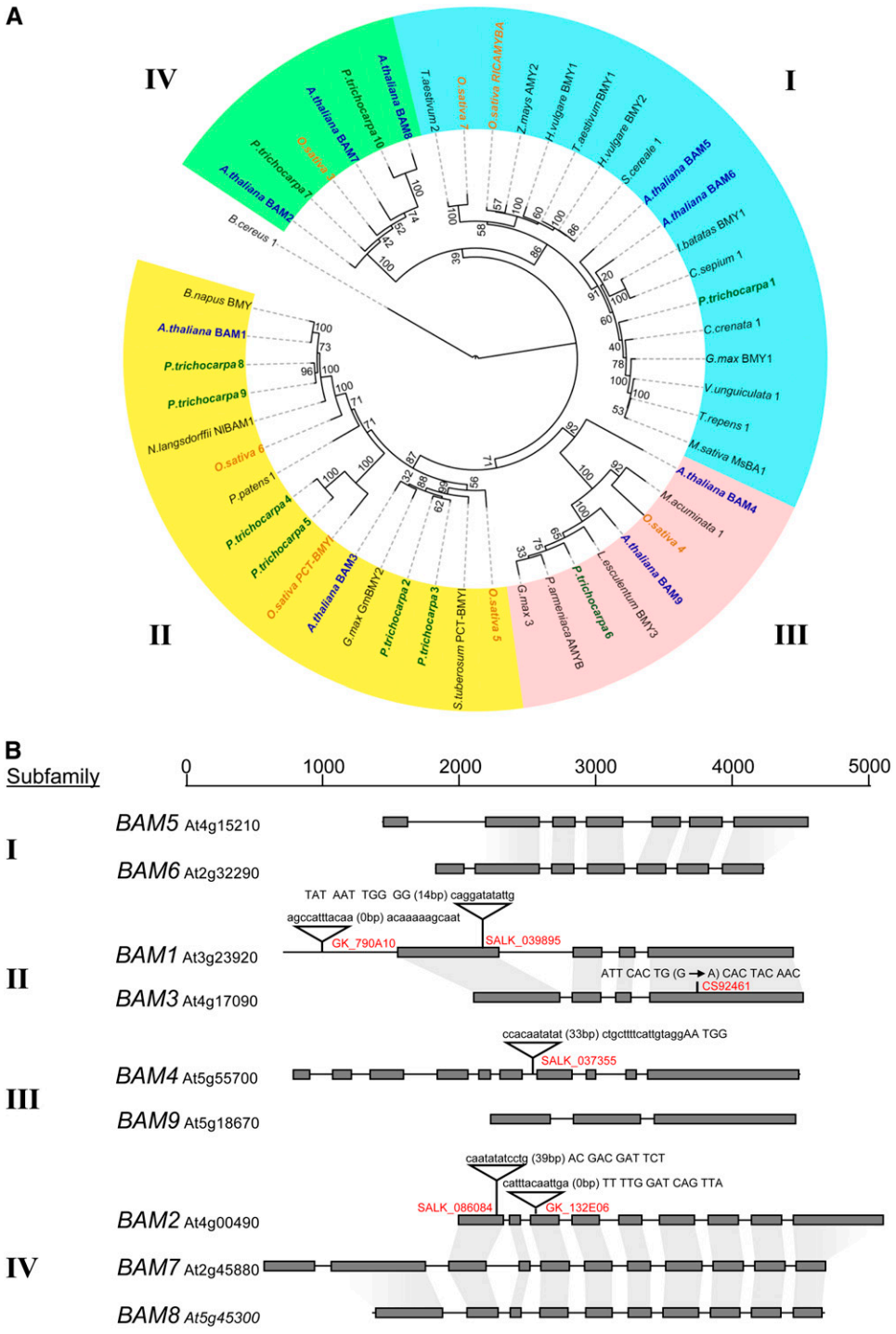

Figure 1. Phylogeny of β-Amylases and the Gene Structure of the *Arabidopsis BAM* Genes.

(A) Phylogram showing that plant β-amylase proteins fall into four families. The core β-amylase domains of 48 plant β-amylases, corresponding to amino acids 17 to 439 of the soybean protein (see Supplemental Table 2 and Supplemental Data Set 1 online), were aligned and used to generate a maximum-likelihood tree displayed using Tree Of Life software (Letunic and Bork, 2007). A prokaryotic β-amylase protein (from *Bacillus cereus*) served as an outlier to root the tree. The robustness of the tree is derived from 100 bootstrap replicates, as shown. *Arabidopsis* proteins are given in blue, rice proteins in orange, and poplar proteins in green.

(B) Gene structure for each of the *Arabidopsis BAM* genes showing the conservation of the intron positions between *BAM5* and *-6*, *BAM1* and *-3*, and *BAM2*, *-7*, and *-8*. The exons are shown as gray boxes, and the scale is shown in base pairs. Triangles show the positions of T-DNA insertions in *bam1*, *bam2*, and *bam4* mutant lines. The insertion site sequences are shown. The T-DNA sequence is given above the insert. The length of sequence that is not derived from either the T-DNA or the *BAM* gene is shown in parentheses. The gene sequence is shown in uppercase (exon) or lowercase (intron or promoter). In the case of *BAM3*, the ethyl methanesulfonate–induced point mutation in exon 4 is shown. Line identifiers are given in red.

candidates for chloroplast localization, and we focused most of our subsequent analyses on these proteins.

We investigated the localization of BAM2, -4, and -8 using two transient expression systems. First, yellow fluorescent protein (YFP) fusion proteins were expressed in *Arabidopsis* leaf mesophyll protoplasts after polyethylene glycol–mediated transfection. Second, green fluorescent protein (GFP) and red fluorescent protein (RFP) fusion proteins were expressed in *Arabidopsis* cultured cells after transformation by biolistic bombardment. In each case, constructs encoded the respective BAM proteins with fluorescent proteins fused to their C termini, and expression was driven by the 35S cauliflower mosaic virus (CaMV) promoter.

For protoplast transformations, constructs encoding BAM1-YFP fusion proteins and free GFP were used as positive controls for chloroplastic and cytosolic localization, respectively. All constructs were used to transfect protoplasts, and after incubation, fluorescence patterns were observed by confocal microscopy. Free GFP localized to the cytosol, as expected (Figure 2A). The fluorescence from BAM2-YFP and BAM4-YFP coincided with the chlorophyll autofluorescence, indicating chloroplastic localizations (Figure 2A). By contrast, the fluorescence from BAM8-YFP did not coincide with the chlorophyll autofluorescence (see Supplemental Figure 1 online). For cell culture biolistic transformations, constructs encoding the small subunit of ribulose-1,5-bis-phosphate carboxylase/oxygenase (Rubisco; from pea [*Pisum sativum*]) (Anderson and Smith, 1986) and BAM3 fused to fluorescent proteins were used as positive controls for plastid localization. After cotransformation with pairs of plasmids encoding GFP- and RFP-labeled proteins, cells were incubated for 24 h and then analyzed by fluorescence microscopy. We observed colocalization of BAM2 and BAM4 with control proteins indicating plastidial localizations. Examples shown here are colocalization of BAM2 with the small subunit of Rubisco and BAM3 with BAM4 (Figure 2B). These results, together with earlier

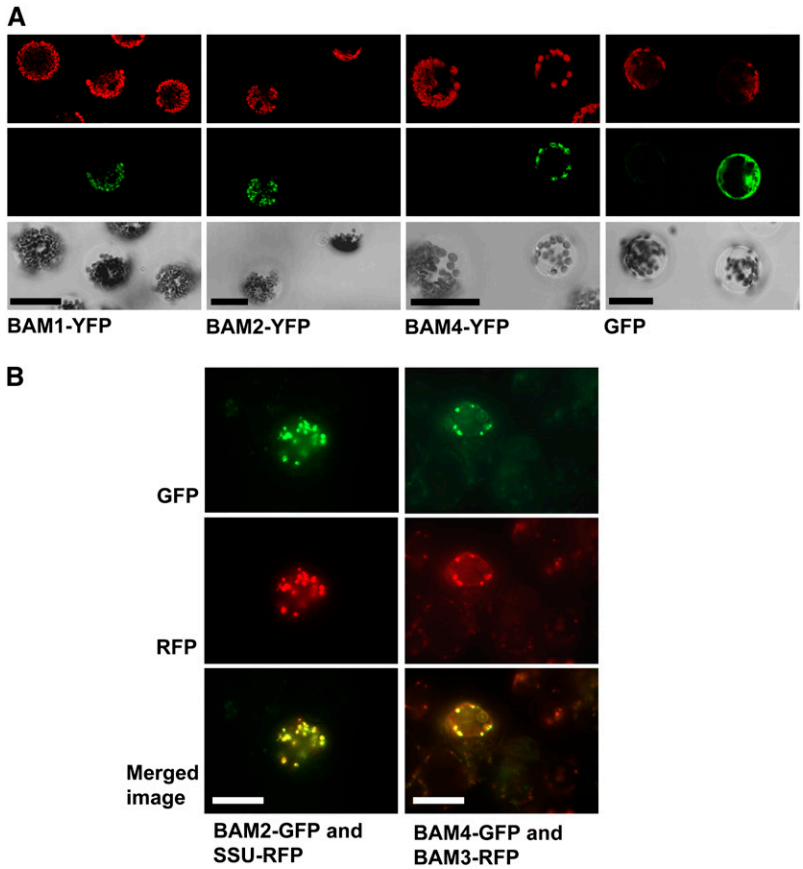

Figure 2. Chloroplast Targeting of BAM2 and BAM4.

(A) Localization of BAM-YFP fusion proteins. Constructs encoding BAM-YFP fusion proteins were transfected into leaf mesophyll protoplasts from wild-type plants. In each case, YFP was fused to the C terminus. Each field of view contains one transfected protoplast and one or more nontransfected protoplasts. Top panels, chlorophyll autofluorescence; middle panels, YFP fluorescence; bottom panels, confocal reflection images of the protoplasts. Note the colocalization of the YFP and the chlorophyll autofluorescence for the three BAM-YFP fusion proteins. Free GFP was used as a cytosol-localized control. Note the difference in pattern between the chlorophyll autofluorescence and free GFP fluorescence. Bars = 50 μm.

(B) Localization of BAM-GFP and BAM-RFP fusion proteins. Cultured *Arabidopsis* cells were cotransformed by biolistic bombardment with constructs encoding BAM proteins or the small subunit of Rubisco (SSU) with either GFP or RFP fused to the C terminus, as indicated. Bars = 50 μm.

experiments revealing the localization of BAM1 and BAM3 (Lao et al., 1999; Sparla et al., 2006), give us confidence that BAM1, -2, -3, and -4 are plastidial proteins.

Expression of BAM1, -2, -3, and -4 in *Escherichia coli*

To study their β-amylase activity, we expressed BAM1, -2, -3, and -4 tagged with glutathione *S*-transferase (GST) at the N-terminal ends in *E. coli*. The design of the constructs involved removal of the transit peptide sequences, based both on predicted cleavage sites and on constructs made successfully for BAM3 (Lao et al., 1999) and BAM1 (Sparla et al., 2006). The resultant proteins were affinity-purified to near homogeneity using Glutathione–Sepharose 4B, and their activity was assayed using *p*-nitrophenyl maltopentoside, a chlorogenic substrate specific for β-amylase. Recombinant BAM1 and BAM3 proteins were active against the substrate (Figure 3A) and displayed a broad pH optimum of 6 to 7, with a steep decline in activity as the pH was increased to 8 (Figure 3C). BAM2 also had a pH optimum of 6, but its specific activity was 25-fold lower than that of BAM3 and 50-fold lower than that of BAM1. No activity was detectable for recombinant BAM4 protein. We made four different BAM4 constructs with different N-terminal ends, one including the transit peptide sequence. All were inactive (data not shown). Removal of the GST tag with thrombin did not affect the activity or properties of any of the enzymes. We also assayed the recombinant BAM3 and BAM4 proteins against potato amylopectin. BAM3 released maltose from amylopectin, whereas BAM4 did not (Figure 3B). This second assay was also used to determine the pH optimum of total β-amylase activity in soluble extracts from wild-type *Arabidopsis* leaves (Figure 3D). Maximal activity was observed between pH 6.0 and 7.0, consistent with the results for the recombinant BAM1 and BAM3 proteins.

Structural Modeling of the BAM4 Active Site Predicts an Inactive Protein

The structures of the soybean β-amylase Gm BMY1 and the sweet potato β-amylase Ib BMY1 have been solved by x-ray crystallography, allowing the substrate binding pocket and the active site to be identified (Mikami et al., 1994; Cheong et al., 1995). Substrate binding is accompanied by movements of an inner loop and a flexible outer loop, and catalysis is mediated by a pair of conserved Glu residues. We aligned the conserved glucosyl hydrolase domains of the *Arabidopsis* proteins with that of the soybean enzyme Gm BMY1. The overall sequence similarity was high (Figure 4). However, the sequences of BAM4 and BAM9 displayed some significant differences from other members of the family. In both cases, there is a substitution of Glu-380, one of the two catalytic residues (marked with red arrowheads in Figure 4, which shows numbering according to the Gm BMY1 protein structure; Protein Data Bank identifier [PDB ID] 1BYB). In BAM4, Glu-380 is changed to Arg, and in BAM9, it is changed to Gln. Mutations of Glu-380 in the soybean enzyme effectively abolish β-amylase activity (Kang et al., 2004).

Both BAM4 and BAM9 are also substituted at position 342 on the inner loop. In the soybean protein, this position is occupied by Thr, which interacts with the catalytic Glu-186 and the substrate. Even conservative substitutions of Thr-342 markedly reduce activity (Kang et al., 2005). Upon glucan binding, the flexible outer loop of the soybean β-amylase moves 10 to 11 Å, forming a substrate tunnel (Mikami et al., 1994). The amino acid sequence of BAM9 has a five–amino acid deletion in the middle of this loop, while the loop sequence in BAM4 is poorly conserved. Further inspection of the subfamily III proteins revealed that, as with BAM4 and BAM9, all are substituted at one or several of the conserved active site residues.

The overall similarity between the β-amylase sequences allowed us to model the active site in more detail. Using the crystal structure of Gm BMY1 with maltotetraose bound (PDB ID 1BYB; Mikami et al., 1994), we identified all residues lining the active site pocket (Figure 4, arrowheads). A direct comparison of the equivalent residues in BAM3 and BAM4 highlighted additional factors that may contribute to the observed inactivity for the BAM4 protein. In the active enzyme BAM3, all but 2 of the 23 amino acids lining the active site are identical to those in Gm BMY1. The first substitution (Ser-297 → Ala) is conservative. The second (Ala-184 → Cys) is readily accommodated in the soybean β-amylase active site in its preferred rotamer orientation without structural clashes with either the glucan or neighboring water molecules (Figures 5A and 5C). By contrast, there are 11 changes in equivalent residues of BAM4. Half of these substitutions are nonconservative (Figure 5E).

The glucan binding pocket of BAM4 predicted from our analysis is smaller, with the change Asp-53 → Glu encroaching on the +2 binding subsite, which would normally accommodate the non-reducing-end residue (the four glucosyl residues occupy the +2, +1, −1, and −2 subsites, and hydrolysis occurs between the residues in positions +1 and −1). Furthermore, the substitutions render the overall electrostatic potential of the binding pocket less electronegative than that of the soybean enzyme and BAM3 (Figures 5B, 5D, and 5F). Collectively, these results provide a plausible explanation for why recombinant BAM4 is inactive (Figure 3A): the data suggest that a critical catalytic residue is mutated in BAM4 and that the protein may have a lower affinity for maltotetraose, which would bind in a different orientation, if at all. Crystallographic studies will be required to confirm these model predictions.

Mutants Deficient in BAM1, -2, -3, and -4

We obtained T-DNA insertion mutations for *BAM1*, *BAM2*, and *BAM4* from the SALK collection (http://signal.salk.edu). In each case, the position of the T-DNA insertion was confirmed by PCR amplification and DNA sequencing (Figure 1B) and homozygous lines were obtained. The T-DNA inserted into the first exon of *BAM1*, the first exon of *BAM2*, and the sixth intron of *BAM4*. Disruption of gene transcription in each case was confirmed by RT-PCR using gene-specific primer pairs spanning the T-DNA insertion site (Figure 6A). The failure to detect the *BAM4* mRNA in the *bam4* mutant shows that the presence of the T-DNA in the intron disrupts mRNA production. For *BAM3*, we obtained a mutant line via the *Arabidopsis* TILLING Program (Till et al., 2003; http://tilling.fhcrc.org:9366/). We confirmed by PCR and DNA sequencing that this line has an ethyl methanesulfonate–induced

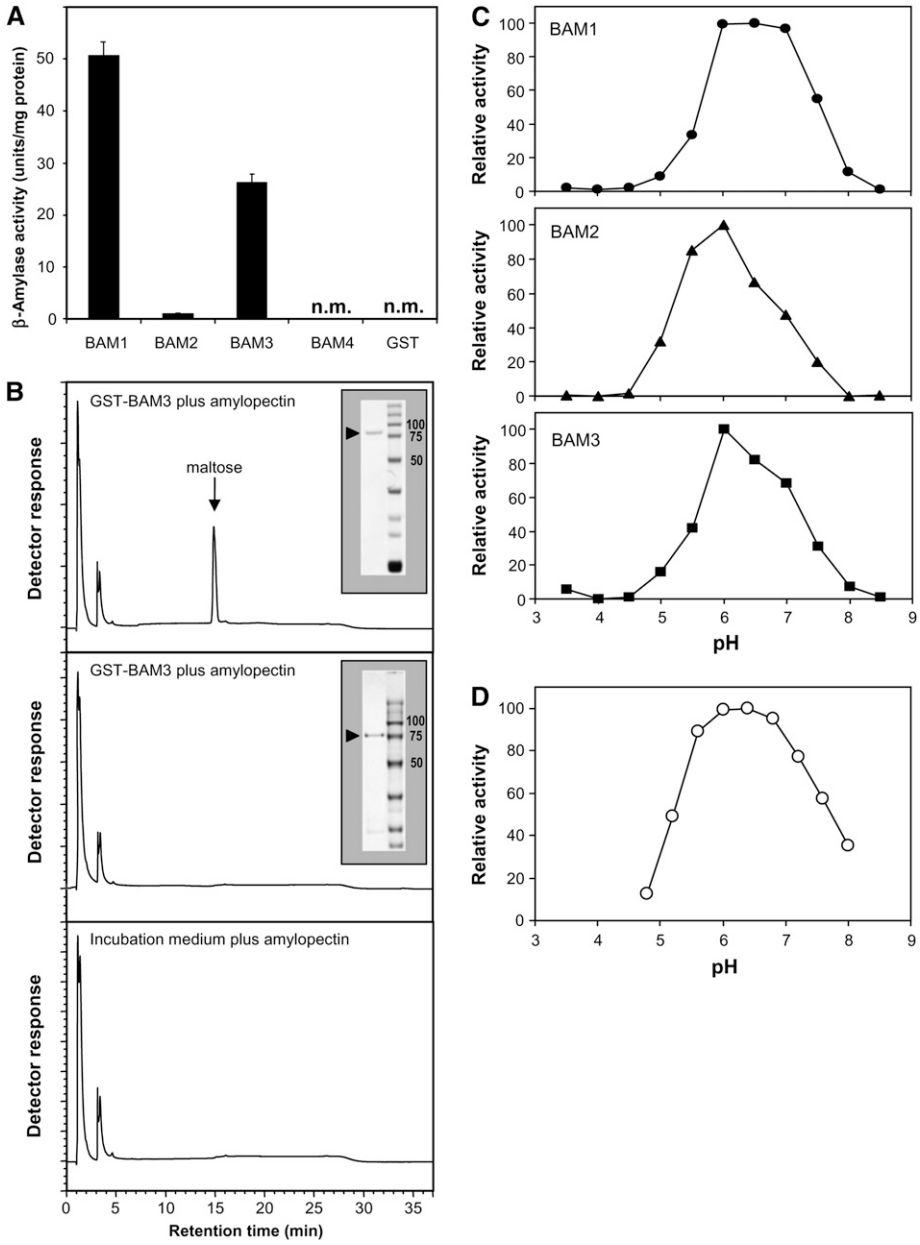

Figure 3. Activity of Recombinant BAM Proteins.

(A) Activity of GST-BAM fusion proteins in *E. coli*. Sequences encoding the chloroplast transit peptides of BAM1, -2, -3, and -4 were removed, and the resultant *BAM* cDNAs were inserted downstream of the GST-coding sequence. Proteins were purified by affinity chromatography, and specific activity was determined using the Betamyl assay kit from Megazyme. Values are means ± SE of measurements made on three replicate protein preparations, each made from an independent *E. coli* culture. Free GST purified in the same way served as a negative control. n.m., no activity measurable.

(B) Activity of affinity-purified GST-BAM3 and GST-BAM4 fusion proteins. Fusion proteins were incubated with amylopectin and assayed for the release of maltose by HPAEC-PAD as described in Methods. The insets in the top and middle panels show SDS-PAGE analysis of recombinant BAM proteins (left lanes), indicated by arrowheads. Molecular mass markers are indicated in kilodaltons (right lanes). The bottom panel shows the control chromatogram, in which no recombinant protein was added.

(C) The pH optima of recombinant BAM1, -2, and -3. The pH optima were determined using the Betamyl assay kit on one of the three protein preparations described for **(A)**. Activity is expressed as a percentage of the maximum value.

(D) The pH optimum for total β-amylase activity in a crude extract of wild-type leaves. The pH optimum was determined by measuring maltose release from amylopectin. Activity is expressed as a percentage of the maximum value.

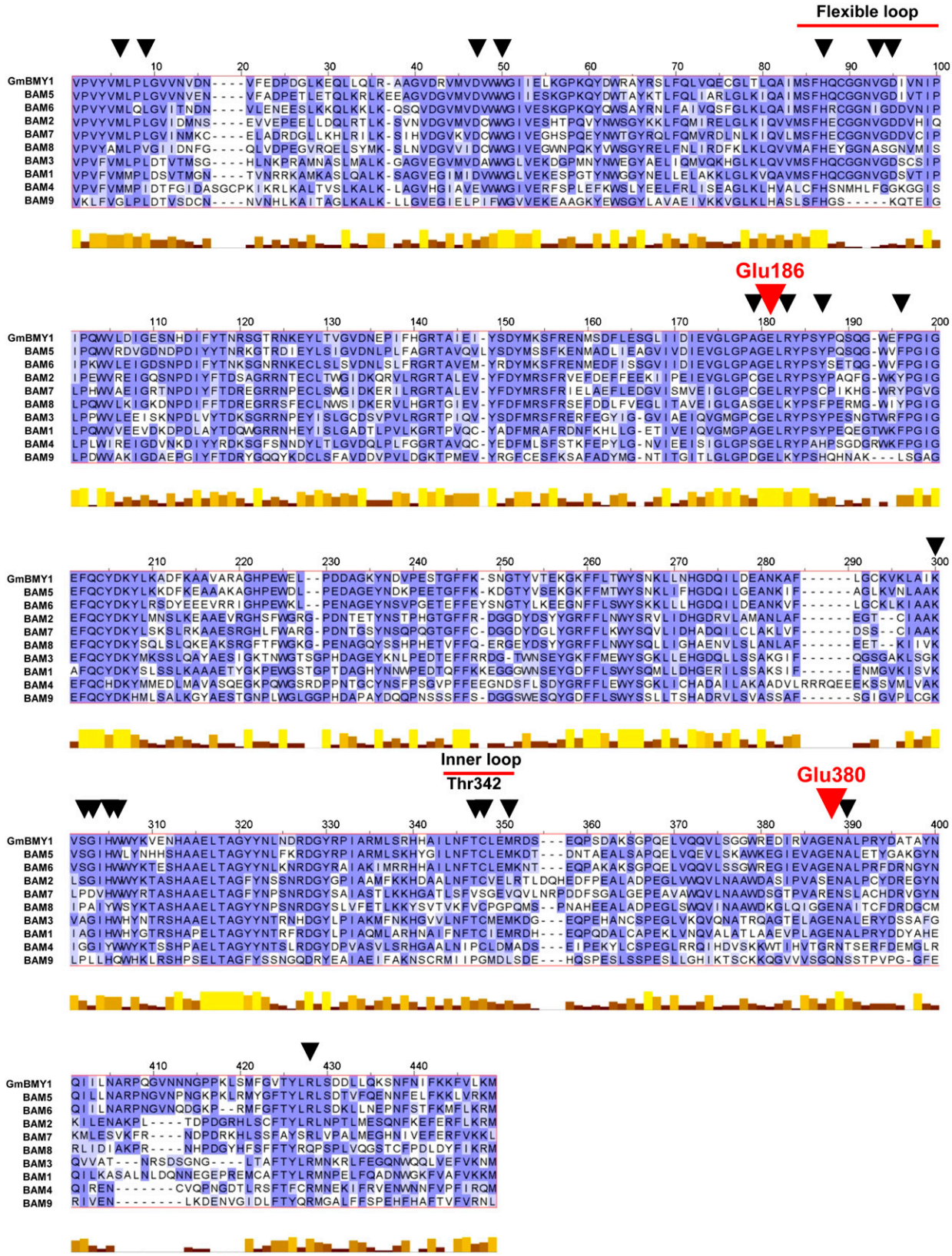

Figure 4. Alignment of the *Arabidopsis* BAM Proteins and the Soybean Gm BMY1 Protein.

point mutation in the fourth exon leading to a premature stop codon in the mRNA (Figure 1B). RT-PCR showed that the mutated *bam3* transcript was still present (Figure 6A).

Total soluble proteins from leaves of the wild type and each of the mutant lines *bam1*, *bam2*, and *bam3* were extracted and separated by SDS-PAGE. Protein gel blots were probed with antisera raised against the recombinant protein (BAM1) and isoform-specific peptides (BAM2 and BAM3). In each of the *bam* mutants, a protein recognized by the appropriate antiserum was missing (Figure 6B). BAM1, BAM2, and BAM3 proteins migrated as 67.5-, 54.6-, and 55.5-kD proteins, respectively. For BAM2 and BAM3, the molecular masses were very close to those predicted (55.5 and 55.8 kD, respectively, after removal of the predicted transit peptide), while for BAM1, the molecular mass was higher than that predicted (59.5 kD). The antiserum to BAM1 also recognized a second protein, of 57 kD, which was also missing in the *bam1* mutant (Figure 6B, gray arrowhead). The BAM2 antiserum also recognized a protein of 56 kD. However, the appearance of this band was inconsistent (see Supplemental Figure 2B online), and since it was unaffected in the *bam2* mutant, we suggest that it is not a product of the *BAM2* gene.

Additional lines with T-DNA insertions in *BAM1* and *BAM2* were obtained from the GABI_KAT collection (http://www.gabi-kat.de/). The positions of the T-DNA insertions were confirmed (Figure 1B), and homozygous lines were identified. The T-DNA inserted into the promoter of *BAM1*, but protein gel blots probed with the BAM1 antiserum revealed that the BAM1 protein was still present (see Supplemental Figure 2A online). The T-DNA insertion in *BAM2* was in the third exon, and protein gel blots probed with the BAM2 antiserum revealed that the BAM2 protein was absent (see Supplemental Figure 2B online). This allele was designated *bam2-2*.

Total β-amylase activity was significantly reduced relative to the wild type in *bam1* and *bam3* leaves but unchanged in *bam2* and *bam4* leaves (Figure 7). Similar results were obtained consistently with different batches of plants grown in both 12-h and 16-h photoperiods. Previously, Laby et al. (2001) reported that *ram1* (a mutant lacking expression of *BAM5*) had almost no β-amylase activity compared with the wild type. Under our growth room conditions, *ram1* and other *bam5* alleles had ~80% of wild-type β-amylase activity (see Supplemental Figure 3 online).

Mutations in *BAM3* and *BAM4* Impair Starch Breakdown

To determine whether the loss of BAM1, -2, -3, or -4 affected starch metabolism, we grew all four mutants and the wild type in a 12-h-light/12-h-dark diurnal cycle in a growth room. The growth rate of *bam1* and *bam2* plants was similar to that of the wild type, whereas that of *bam3* and *bam4* was slightly retarded (Figure 8A). We stained the plants for the presence of starch at the end of the night, when wild-type plants have normally exhausted their starch reserves. *bam3* and *bam4* leaves still contained starch, whereas starch was not detected in the leaves of *bam1*, *bam2* (either allele), or the wild type (Figure 8B; see Supplemental Figure 2C online). These results suggest that both BAM3 and BAM4 are required for normal starch breakdown. Our result for the *bam4* mutant is intriguing considering that the activity measurements (Figure 3A) and structural modeling (Figures 4 and 5) suggest that BAM4 is not an active β-amylase. To confirm that the effect on starch metabolism in *bam4* is the direct result of the loss of the BAM4 protein, we transformed the *bam4* mutant with a construct containing the *BAM4* promoter sequence linked to the *BAM4* cDNA. Transformed plants regained the capacity to degrade essentially all of their starch (see Supplemental Figure 4 online).

Since *bam3* and *bam4* both had elevated starch levels, we produced the *bam3 bam4* double mutant to test for epistasis. The *bam3* and *bam4* mutants both synthesized starch during the day and degraded it during the night, but they had elevated levels with respect to the wild type throughout the diurnal cycle (Figure 8C). The *bam3 bam4* double mutant also synthesized and degraded starch during the diurnal cycle, but the elevated starch phenotype was more severe than in the single mutants. Diurnal maltose levels were significantly altered in the mutants. In the wild type, the maltose content of the leaves increased rapidly at the start of the night, peaked at 4 h into the night period, and then declined toward the end of the night (Figure 8D). In the mutants, the maltose content increased more slowly at the start of the night and levels remained lower than in the wild type in the first 8 h of the night. The reduction was modest in *bam4*, greater in *bam3*, and greatest in *bam3 bam4*.

These data suggest that the rate of maltose production in each of the mutants—hence, the rate of starch degradation—is reduced relative to the wild type. Interestingly, the maltose levels at the end of the night were higher in the mutants than in the wild type. We suggest that in the wild type, starch reserves become depleted toward the end of the night and maltose production declines. In the mutants, the elevated starch levels mean that maltose production can continue until the end of the night. At the start of the day, maltose levels declined to low levels in all four lines. However, at each point during the day, the *bam3* mutant had significantly more maltose than the wild type (Figure 8D, inset). This observation was reproducible in other batches of independently grown plants (see Figure 10A).

Figure 4. (continued).

The alignment was made using the ClustalW sequence alignment program and analyzed using Jalview (Clamp et al., 2004). Criteria for calculating overall levels of sequence conservation are based on those described for the program AMAS (Analyze Multiply Aligned Sequences; Livingstone and Barton, 1993). Dark and light blue shading indicate identical residues and conservative substitutions, respectively. Unshaded residues are not conserved. The bar graph below gives an overall picture of sequence conservation, with tall yellow bars representing high sequence conservation and short brown bars representing low sequence conservation. Black arrowheads indicate substrate binding residues. Larger red arrowheads indicate the two catalytic residues. Note the lack of conservation in the flexible loop structure in BAM4 and BAM9. The aligned protein sequences are available as Supplemental Data Set 2 online.

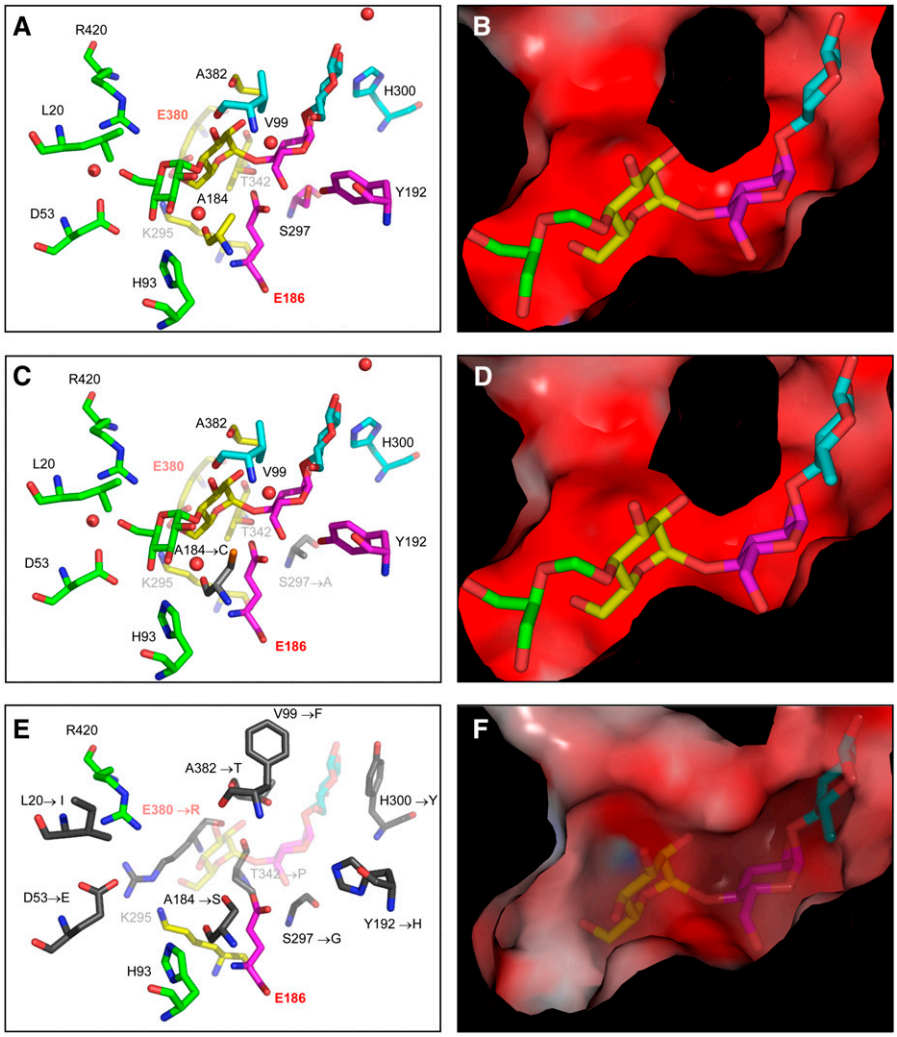

Figure 5. Structural Modeling of the Active Sites of BAM3 and BAM4.

Modeling of BAM3 and BAM4 was conducted by substituting amino acids lining the active site of soybean β-amylase Gm BMY1 (PDB ID 1BYB) with the equivalent amino acids found in BAM3 and BAM4.

(A) Stick representation of the amino acids of the Gm BMY1 active site with maltotetraose bound, as determined by Mikami et al. (1994). The four glucosyl residues are colored green, yellow, purple, and cyan, with the green residue being at the nonreducing end of the chain. Amino acids are colored according to the glucosyl residue with which they interact. For clarity, not all amino acid residues are shown. Catalytic residues are labeled in red. Red spheres indicate water molecules.

(B) Cut-away view of the active site of Gm BMY1. Maltotetraose is shown as in **(A)**. Not all atoms of the glucan are shown due to the plane of the section. The surface of the binding site is colored according to electrostatic potential (from −10 [red] to +10 kT/e [blue]).The binding pocket is very negatively charged.

(C) Stick representation of the amino acids of the modeled BAM3 active site with maltotetraose bound. The structural features are as in **(A)**. Residues that are not conserved between the two proteins are indicated and shown in gray.

(D) Cut-away view of the modeled active site of BAM3. Structural features are as described for **(B)**. The binding pocket of BAM3 is very similar to that of Gm BMY1.

(E) Stick representation of the amino acids of the modeled BAM4 active site. The structural features are as in **(A)**, but maltotriose is shown as maltotetraose would not fit into the modeled active site in the same orientation as in the soybean protein. The nonreducing end residue is shown in yellow. Note the abundance of gray, nonconserved amino acid residues, including the catalytic residue Glu-380.

(F) Cut-away view of the modeled active site of BAM4. Structural features are as described for **(B)**. A stick model of maltotriose is shown. This modeled binding pocket is considerably less polar (white surface) than the active site of Gm BMY1 and that modeled for BAM3.

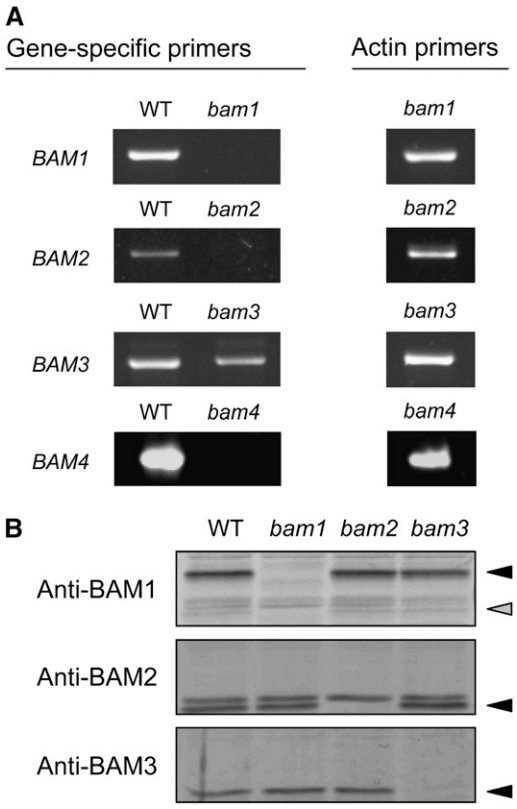

Figure 6. Identification of *bam* Mutants.

(A) Analysis of *Arabidopsis* lines carrying mutations in *BAM1*, *-2*, *-3*, and *-4* using RT-PCR. Primers annealing to sequences on either side of the T-DNA insertion site given in Figure 1B amplified the correct cDNA sequences in the wild type. In *bam1*, *bam2*, and *bam4*, the presence of the T-DNA abolishes expression. In *bam3*, the nonsense transcript is still expressed. Primers annealing to the Actin2 cDNA were used as a positive control.

(B) Separation of proteins in crude extracts of leaves of the wild type and the *bam1*, *bam2*, and *bam3* mutants using SDS-PAGE. Antisera recognizing BAM1, BAM2, or BAM3 were used to probe protein gel blots. Each panel shows proteins between 50 and 75 kD in size. Each antiserum recognized a protein in the wild type that was missing in the corresponding mutant (black arrowheads). The antiserum to BAM1 also recognized a faint, lower molecular weight band (gray arrowhead). A replicate blot yielded the same result.

BAM1 Is Necessary for Starch Breakdown in the Absence of BAM3

We constructed all of the double, triple, and quadruple mutant combinations between the four *bam* single mutants and conducted a series of experiments to compare their starch and maltose contents. Since it was not possible to compare all 16 genotypes in a single experiment, we performed several experiments. The growth conditions were the same in each case. The genotype selections for each experiment overlapped to control for small growth and technical variations and always included the wild type (see legends of Figures 9 and 10).

The results of these experiments indicate that the 15 different mutant combinations fall into six phenotypic categories: that of the wild type and five progressively more severe phenotypes with increased levels of leaf starch and decreased nighttime levels of maltose (Figures 9 and 10). (1) The *bam1* and *bam2* mutants, and the *bam1 bam2* double mutant, all have the wild-type phenotype. (2) The *bam4* mutant has a mild phenotype with increased starch and decreased nighttime maltose. The additional loss of BAM1 and/or BAM2 does not affect this phenotype appreciably, as *bam1 bam4*, *bam2 bam4*, and *bam1 bam2 bam4* are all similar to *bam4*. (3) The *bam3* mutant has a slightly more severe phenotype, with higher levels of starch and lower levels of maltose than *bam4*. The additional loss of BAM2 in the *bam2 bam3* double mutant does not affect the phenotype appreciably. (4) The *bam3 bam4* double mutant phenotype is more severe than that of either of the single mutants (Figures 8 to 10). Again, additional loss of BAM2 in the *bam2 bam3 bam4* triple mutant has no additional effect. (5) Loss of both BAM1 and BAM3 (the *bam1 bam3* double mutant) leads to a severe phenotype, showing that when BAM3 is missing, BAM1 contributes to starch degradation and maltose production at night. The phenotype of the *bam1 bam2 bam3* triple mutant is similar to that of *bam1 bam3*. (6) The simultaneous loss of BAM1, BAM3, and BAM4 (the *bam1 bam3 bam4* triple mutant) results in the most severe phenotype, which is shared by the quadruple mutant. These findings are summarized in Figure 9B, which shows the impact on starch levels of the loss of a given BAM protein, using data from all of the mutant backgrounds. Loss of BAM3 and BAM4 always results in increased starch accumulation. In the case of BAM3, this effect is less severe if BAM1 is present. Loss of BAM1 has no effect if BAM3 is present but has a major impact if BAM3 is also missing. The loss of BAM2 has little effect in any of the genetic backgrounds analyzed.

As expected, an increase in starch levels inversely correlates with the nighttime levels of maltose (Figure 10B). Despite the

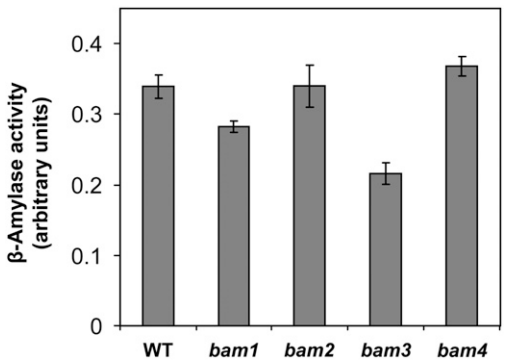

Figure 7. β-Amylase Activity in *bam* Mutants.

Total β-amylase activity in crude extracts from leaves of the wild type and the four single *bam* mutants was determined using the Betamyl assay kit from Megazyme. Each sample comprised two to four mature leaves from an individual plant. Values are means ± SE from five replicate samples. Replicate experiments with separate batches of plants gave comparable results.

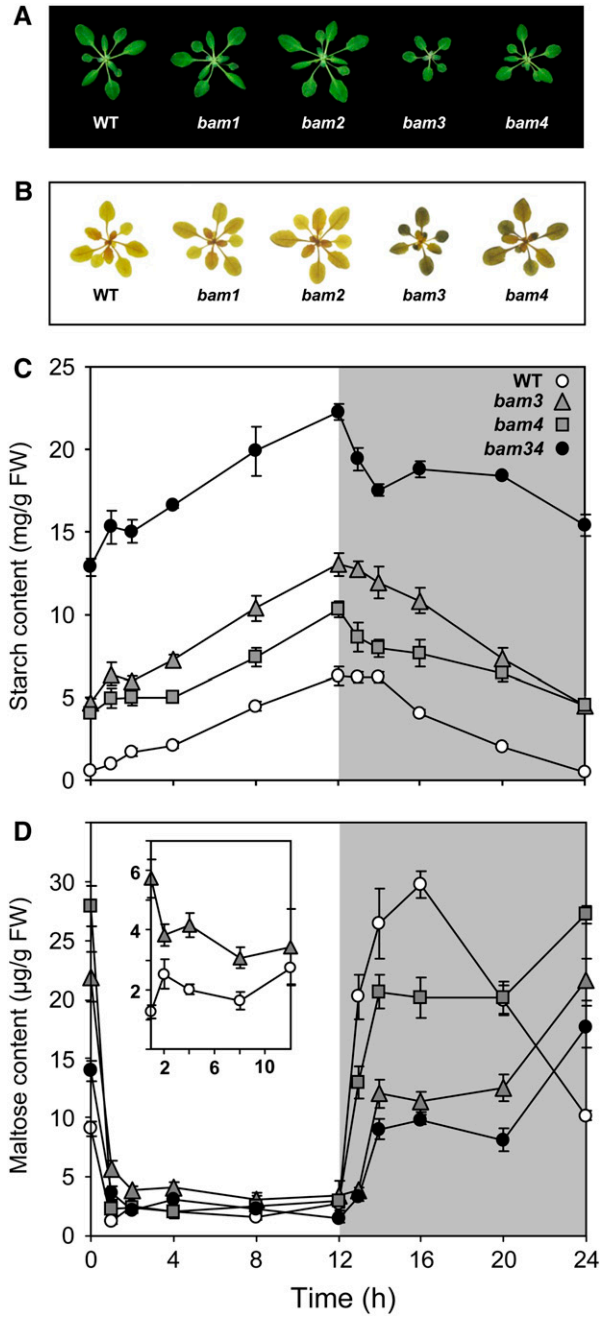

Figure 8. Elevated Starch Phenotype of *bam3* and *bam4* Single Mutants and Diurnal Changes in Starch and Maltose Contents.

(A) Photographs of wild-type and *bam* mutant plants harvested after 5 weeks of growth. Representative plants were selected to show the reduced growth rate of *bam3* and *bam4* mutants.

(B) Starch content in 5-week-old wild-type and *bam* mutant plants harvested at the end of the night. Plants were decolorized in hot 80% (v/v) ethanol and stained for starch with iodine solution.

(C) Leaf starch content throughout the diurnal cycle in the wild type, *bam3*, *bam4*, and the *bam3 bam4* double mutant. Each sample comprised all of the leaves of an individual plant. Each value is the mean ± SE of five replicate samples. FW, fresh weight.

(D) Leaf maltose content throughout the diurnal cycle in the wild type, *bam3*, *bam4*, and the *bam3 bam4* double mutant. Plants were the same as those in **(C)**, as indicated. Each value is the mean ± SE of five replicate samples. The inset shows a comparison of daytime maltose levels in the wild type and in the *bam3* mutant.

severity of the phenotype of the quadruple mutant, some starch is still broken down during the night (Figure 9A) and some maltose is still produced (Figure 10A). This indicates that either another β-amylase or a different enzyme produces maltose in the quadruple mutant. Previously, we showed that in mutants deficient in starch-debranching enzymes, the chloroplastic α-amylase AMY3 was induced and intermediates consistent with α-amylolytic starch breakdown accumulated (Delatte et al., 2006). Measurements of total α-amylase activity revealed only slight increases (15 to 25%) in the *bam3*, *bam4*, *bam3 bam4*, and quadruple *bam* mutant (see Supplemental Figure 5A online), and protein gel blots of crude extracts of leaves did not reveal an increase in the amount of the chloroplastic α-amylase, AMY3 (see Supplemental Figure 5B online). Malto-oligosaccharides longer than maltose, which could be produced by α-amylolysis and debranching, were still detectable in the quadruple mutant at levels comparable to those in the wild type (data not shown).

DISCUSSION

Our study reveals that BAMs play a central role in the breakdown of leaf starch. It also reveals a surprising level of complexity in terms of specialization within the β-amylase gene family as well as a potential facilitatory or regulatory role played by at least one catalytically inactive member. Multiple β-amylase proteins, which fall into the same phylogenetic families as the *Arabidopsis* proteins, are also encoded by the genomes of rice and poplar (Figure 1A). This suggests that the complexity of β-amylase function is a general feature of higher plants and not specific to *Arabidopsis*. β-Amylases directly involved in starch breakdown must be localized in the chloroplast. We confirmed experimentally that BAM1, -2, -3, and -4 were all targeted to the chloroplast. However, we do not rule out the possibility that some of the remaining BAM proteins are also targeted to the chloroplast, either via transit peptides that are not recognized by the prediction algorithms or via an alternative route (e.g., the endoplasmic reticulum) (Asatsuma et al., 2005; Villarejo et al., 2005). This could account for the residual starch degradation and maltose production in the quadruple *bam* mutant.

BAM1 and BAM3 Both Contribute to Starch Breakdown

BAM1 and *BAM3* encode active chloroplastic β-amylases (Kaplan and Guy, 2005; Sparla et al., 2006) (Figure 3A) that fall within the same β-amylase subfamily (Figure 1A). Both are expressed in leaves (Smith et al., 2004) (Figure 6), and *bam1* and *bam3* mutants have reduced total β-amylase activities (Figure 7). The fact that both *BAM1* and *BAM3* have orthologs in rice and poplar suggests that the presence of multiple active chloroplastic β-amylases is widespread in higher plants. Of the

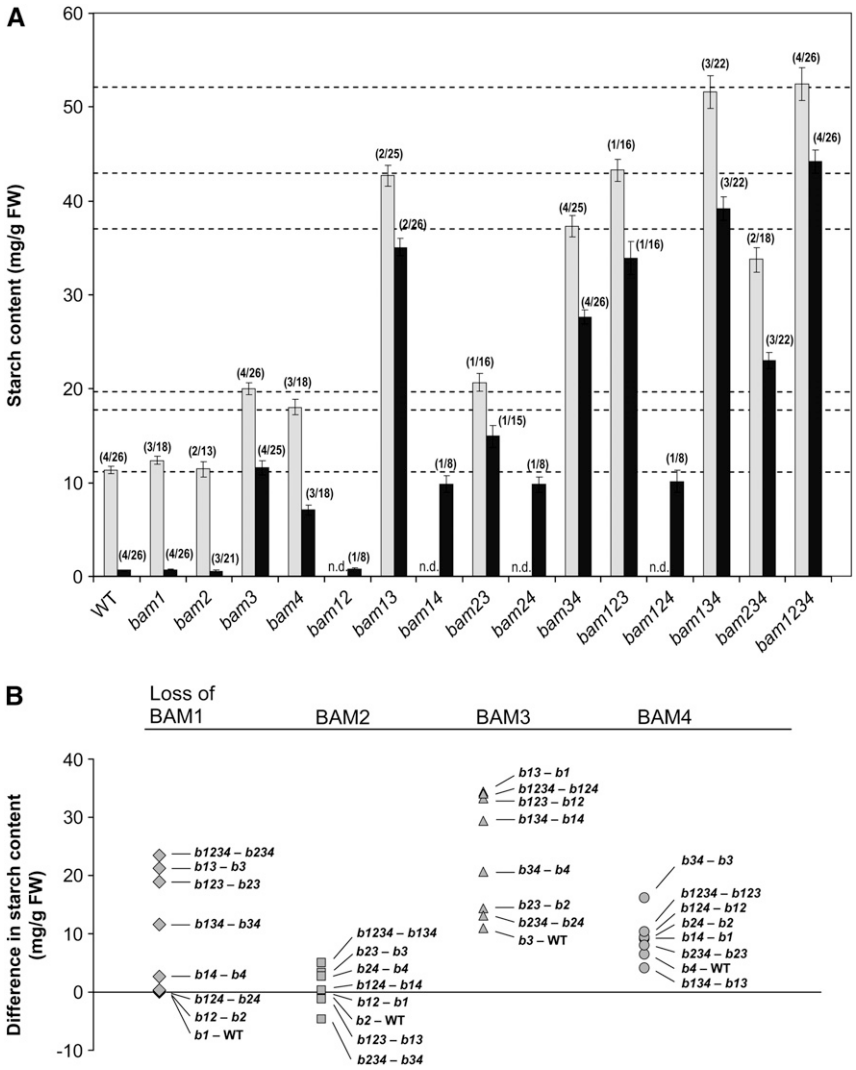

Figure 9. Impact on Leaf Starch Content of Single Mutations in *BAM1*, *-2*, *-3*, and *-4* and of Multiple Mutant Combinations.

(A) Starch content of the aerial parts of individual plants harvested at the end of the day (light bars) and the end of the night (dark bars). Measurements of samples from four independently grown batches of plants are combined (not including the plants shown in Figure 8). Values are means ± SE. The values in parentheses above each bar show the number of replicate plants (right) and the number of plant batches (left) from which the samples were taken. Dashed lines indicate the end-of-day starch content of the different phenotypic classes, corresponding to the wild type, *bam4*, *bam3*, *bam3 bam4*, *bam1 bam3*, and *bam1 bam3 bam4* (see text). FW, fresh weight; n.d., not determined.

(B) Impact on leaf starch content of the loss of individual BAM proteins in different genetic backgrounds. Starch values from the end of the night (shown in **[A]**) were subtracted as indicated. Note that the loss of BAM3 or BAM4 always causes an increase in starch content, regardless of the presence or absence of the other BAM proteins. Loss of BAM1 has a major impact only if BAM3 is already missing. Loss of BAM2 has little impact.

two proteins, BAM3 appears to be the dominant isoform in starch degradation, as the *bam3* mutant displays a starch-excess phenotype and has reduced levels of maltose at night. Similar results have been obtained through the repression of *BAM3* expression in *Arabidopsis* (Kaplan and Guy, 2005) and its ortholog in potato (Scheidig et al., 2002). By contrast, *bam1* single mutants are indistinguishable from the wild type (Kaplan and Guy, 2005; this study). However, the increased severity of the starch-excess phenotype of the *bam1 bam3* double mutant shows that the two enzymes have overlapping functions and that, at least in the absence of BAM3, BAM1 does contribute to starch breakdown.

The functional significance of the conservation of two active isoforms is not yet clear. One possibility is that they are differentially regulated such that starch degradation can be induced by different signals. For example, *BAM3* expression is strongly induced by cold (Kaplan and Guy, 2005), during which starch degradation provides soluble sugars that help the plant to tolerate the stress (Kaplan et al., 2006, and references therein). *BAM1* expression is not induced by cold stress, but analysis of

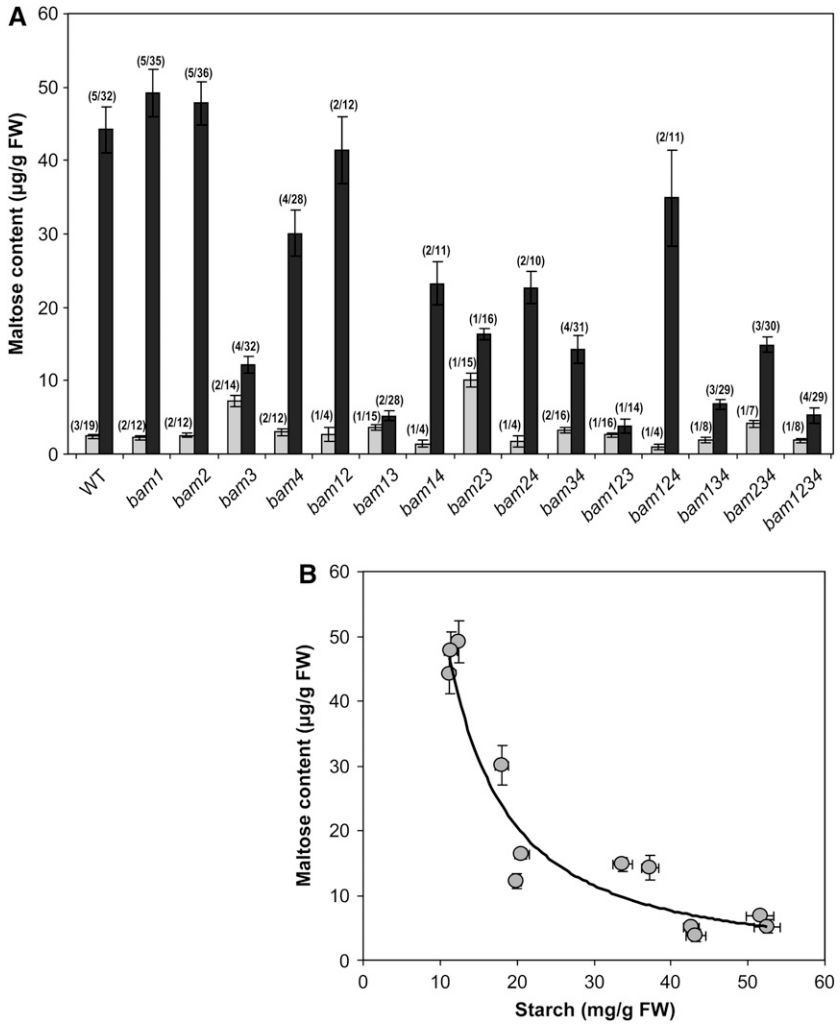

Figure 10. Impact on Leaf Maltose Content of Single Mutations in *BAM1*, *-2*, *-3*, and *-4* and of Multiple Mutant Combinations.

(A) Maltose content of the aerial parts of individual plants harvested at 4 h into the day (light bars) and 4 h into the night (dark bars). Measurements of samples from five independently grown batches of plants are combined (not including the plants shown in Figure 8). Values are means ± SE. The values in parentheses above each bar show the number of replicate plants (right) and the number of plant batches (left) from which the samples were taken. FW, fresh weight.

(B) The relationship between starch content at the end of the day (Figure 9A) and maltose content at 4 h into the night (**[A]**). A power-function trend line is plotted (Microsoft Excel).

microarray data shows that it is induced by other treatments, including heat stress, osmotic stress, and oxidative stress. The BAM1 protein is also reported to be activated via thioredoxin-mediated reduction (Sparla et al., 2006). Such regulation is generally associated with the changes in stromal redox potential driven by the photosynthetic electron transport chain via the electron carrier ferrodoxin (Buchanan and Balmer, 2005). On the one hand, redox regulation of starch breakdown is counterintuitive, as chloroplastic thioredoxins are presumed to be more reduced during the day, when starch is synthesized, and more oxidized during the night, when starch is being degraded. On the other hand, there may be circumstances in which starch breakdown during the light is advantageous (e.g., during photorespiratory conditions [Weise et al., 2006]). It is also possible that BAM1 could be activated at night through NADPH-dependent thioredoxin-mediated regulation (Serrato et al., 2004).

Interestingly, we observed that the daytime levels of maltose, although much lower than the levels during the night, were elevated in the *bam3* mutant relative to the wild type (Figures 8D and 10A). This might indicate that in *bam3* BAM1 is activated during the day and produces maltose. However, BAM1 must also be active at night, as the nighttime maltose levels were lower in the *bam1 bam3* double mutant than in the *bam3* single mutant (Figure 10A). Thus, it is possible that BAM1 may be redox-activated independently of light. A precedent for this was provided recently by the redox activation of ADPglucose pyrophosphorylase in darkened chloroplasts in response to the signal metabolite trehalose-6-phosphate (Kolbe et al., 2005).

BAM2 Has No Discernible Function

Our data do not reveal a role for BAM2. The recombinant enzyme is active, but its specific activity is 25 to 50 times lower than that of BAM1 or BAM3. In the *bam2* mutant, there was no reduction in total β-amylase activity and the plants were not distinguishable from wild-type plants. The loss of BAM2 alone, or in addition to any of the other BAMs examined here, did not affect the phenotypes we analyzed (Figures 9 and 10). Together, these data imply that BAM2 does not play a significant role in the breakdown of starch under our growth conditions. BAM2 falls into subfamily IV with BAM7 and BAM8 and is likely to be a duplicate of BAM7. However, BAM2 is shorter at its N terminus than BAM7 and BAM8 and the predicted rice and poplar proteins that fall into subfamily IV. On this basis, we suggest that BAM2 has undergone a partial gene deletion, which may have resulted in the creation of a cryptic chloroplast transit peptide.

Does BAM4 Play a Facilitatory or Regulatory Role in Starch Breakdown?

BAM4 plays an important role in starch breakdown, but unlike BAM1, -2, and -3, no β-amylase activity could be attributed to it (Figure 3). There are two possible explanations for our results. It is possible that BAM4 is a catalytically active protein, but the conditions used for the measurement of β-amylase activity may not have been appropriate to detect it. Such a situation could arise for a number of reasons: BAM4 may have a very specific substrate or require cofactors or protein partners that were not present in our assay mixtures. It is possible that the protein expressed in *E. coli* is not correctly folded or lacks posttranslational modifications. If BAM4 is active in vivo, the elevated starch content in lines carrying the *bam4* mutation could be attributed simply to a reduced capacity to catalyze the hydrolysis of glucans, as proposed for BAM3 and BAM1. However, based on the amino acid substitutions in the active site (Figures 4 and 5), we consider this to be an unlikely explanation. We suggest that BAM4 is catalytically inactive but may have a distinct facilitatory or regulatory function in starch metabolism.

We speculate that BAM4 may act through interactions with other proteins to stimulate starch breakdown. In the absence of BAM4, breakdown is not enabled; thus, maltose levels are lower and starch levels are elevated. For example, BAM4 might be a subunit of a heteromultimeric β-amylase containing other active BAM subunits. Precedents for such a configuration include the starch-debranching enzyme isoamylase (ISA), which contains catalytic ISA1 subunits and related but noncatalytic ISA2 subunits (Hussain et al., 2003; Delatte et al., 2005; Wattebled et al.,

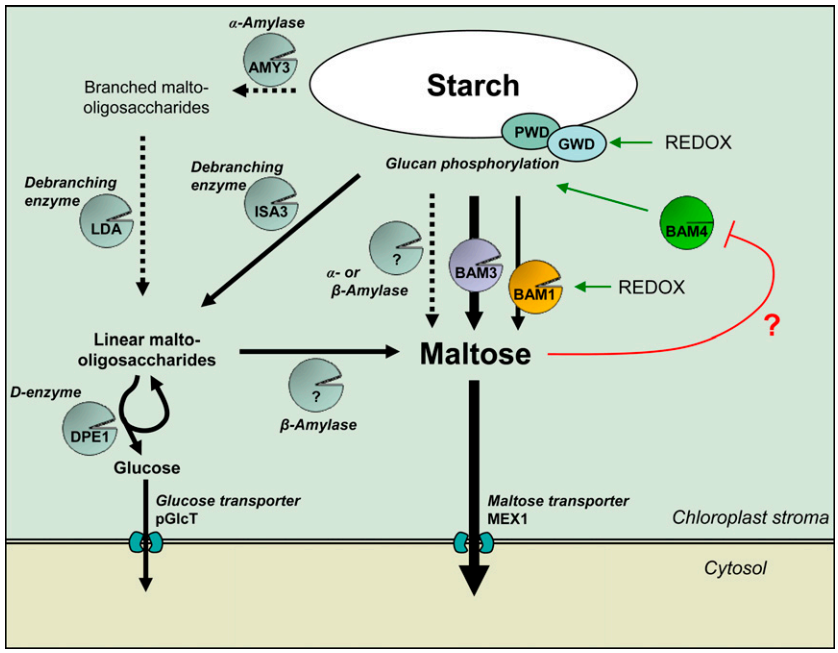

Figure 11. Model Integrating the Roles of the Different BAM Proteins into the Pathway of Starch Degradation.

This model places BAM3 at the heart of starch degradation. BAM1 plays an overlapping role with BAM3. Our data indicate that additional α- or β-amylases may also contribute to starch degradation. Linear malto-oligosaccharides released by the combination of α-amylase and the debranching enzymes ISA3 and LDA (Delatte et al., 2006), or through the action of disproportionating enzyme (D-enzyme DPE1; Critchley et al., 2001), may also provide substrates for the β-amylases. The model proposes that BAM4 acts in a regulatory capacity, upstream of BAM1 and BAM3. A possible target area for regulation could be the process of glucan phosphorylation, mediated by glucan, water dikinase (GWD; Yu et al., 2001) and phosphoglucan, water dikinase (PWD; Baunsgaard et al., 2005; Kötting et al., 2005). GWD activity, like that of BAM1, is reported to be redox-regulated (Mikkelsen et al., 2005; Sparla et al., 2006). We speculate that maltose levels might modulate the action of BAM4, although this remains to be tested experimentally.

2005; Utsumi and Nakamura, 2006), and ADPglucose pyrophosphorylase, which can also be composed of a catalytic subunit and a related noncatalytic subunit (Smith-White and Preiss, 1992). However, total β-amylase activity in the *bam4* mutant is unaltered (Figure 7), arguing against such a role. Furthermore, the loss of BAM4 in addition to BAM3, or to BAM1 and BAM3, increases the severity of the starch-excess phenotype. This implies that BAM4 does not exert its effect over the pathway by acting directly through BAM1 or BAM3.

An alternative possibility is that BAM4 interacts with another enzyme necessary for starch granule degradation. It was shown recently that the activities of recombinant BAM1 and BAM3 on isolated starch granules are stimulated by glucan, water dikinase–mediated phosphorylation of the granule surface (Edner et al., 2007). This effect was enhanced by the addition of the debranching enzyme ISA3 (Edner et al., 2007). Interaction of BAM4 with either glucan, water dikinase or ISA3 to promote or facilitate their activities could explain why the loss of BAM4 results in a starch-excess phenotype independently of BAM1 and BAM3. It is also tempting to speculate that BAM4 retains the ability to bind a glucan (e.g., maltose), which might modulate its proposed interactions with other proteins. Excess maltose could inhibit BAM4 function, creating a negative-feedback system whereby maltose levels in the plastid could influence the rate of further maltose production. In this case, BAM4 would be a regulator of the rate of degradation. However, further studies are required to evaluate these hypotheses and determine the precise role of BAM4. Interestingly, ESTs of genes encoding subfamily III proteins from various species have been isolated from both photosynthetic tissues (leaves and stems) and nonphotosynthetic tissues (roots and developing and mature fruits). This suggests that BAM4-like proteins may also be important in regulating starch metabolism in heterotrophic tissues.

A model of the core components of starch breakdown in *Arabidopsis* leaves incorporating the conclusions of this work is shown in Figure 11. The model reflects the fact that there is likely to be another maltogenic activity (either an α-amylase or another chloroplast-targeted β-amylase) in addition to BAM1, -2, and -3. This is indicated by the continued starch degradation and maltose production in the quadruple *bam* mutant during the night (Figure 10A). The model also reflects the possibility that β-amylase may attack both the starch granule itself and soluble, linear glucans produced by α-amylolysis and disproportionation reactions. Different BAM isoforms may have different substrate specificities, some preferentially attacking soluble linear glucans and others attacking the starch granule directly. Understanding the molecular mechanisms that control starch metabolism has profound implications for identifying rational approaches to regulating plant growth, responses to stress, and energy production in crops. We conclude that β-amylase family members play a central role in such mechanisms.

METHODS

Plant Material and Growth Conditions

Arabidopsis thaliana plants (ecotype Columbia) were grown in a nutrient-rich, medium-grade, peat-based compost in a Percival AR95 growth chamber (CLF Plant Climatics) at a constant temperature of 20°C, 70% RH, with either a 12-h or 16-h photoperiod. The light intensity was uniform at 150 $\mu mol \cdot m^{-2} \cdot s^{-1}$. Seeds were sown by hand. After seedling establishment, individuals were pricked out into 200-mL pots. T-DNA insertion mutant lines from the Salk Institute and the GABI-Kat project (Max Plank Institute for Plant Breeding Research) and TILLING lines from the *Arabidopsis* TILLING Program were obtained via the European *Arabidopsis* Stock Centre. Identifying numbers for these lines are presented in Figure 1. TILLING lines were backcrossed to the wild type, and the mutant was reselected from the F2 generation. *Arabidopsis* suspension cells were maintained as described by Millar et al. (2001).

Phylogenetic Analysis of Plant β-Amylases

A selection of plant β-amylase protein sequences (see Supplemental Table 2 online) was obtained from public databases. The *Bacillus cereus* β-amylase protein sequence was used as an outlier to root the phylogenetic tree. A multiple sequence alignment of the core glucosyl hydrolase domains (~420 amino acids) was built using MUSCLE (Edgar, 2004) with default settings, with the maximum number of iterations set to 100. We then inferred a maximum-likelihood phylogenetic gene tree using PHYML (Guindon and Gascuel, 2003) with the JTT matrix (Jones et al., 1992). As a starting topology for the maximum-likelihood tree search, we reconstructed a variance-weighted least-squares tree using the PhylogeneticTree function implemented in Darwin (Gonnet et al., 2000). In our model of sequence evolution, we assumed two classes of sites, invariable and variable. The variation of rates across the variable sites was modeled by a γ distribution approximated discretely with eight categories of sites. The robustness of the estimated maximum-likelihood tree with regard to small changes in the data was evaluated using 100 bootstrap replicates.

Structural Modeling

To align the glucosyl hydrolase domain of BAM1 to BAM9 with the soybean (*Glycine max*) β-amylase, we used the ClustalW sequence alignment program (European Biofinformatics Institute web interface; http://www.ebi.ac.uk/Tools/clustalw2/) using the default settings together with Jalview (Clamp et al., 2004). The crystal structure of the soybean β-amylase (PDB ID 1BYB) was used for all structural analysis. Residues and water molecules within 3.9 Å of the maltotetraose moiety were designated as lining the active site pocket of 1BYB and were determined using CONTACT (Collaborative Computational Project, Number 4, 1994). Equivalent amino acids in BAM3 and BAM4 were determined using the sequence alignment. Amino acid substitutions were made in PyMOL (DeLano, 2002). For residues in which substitution of the most preferred rotamer resulted in a structural clash with other residues, other rotamer positions were considered; the one causing the fewest unfavorable interactions was chosen by visual inspection. Surface electrostatic potential was calculated using APBS (Baker et al., 2001) and visualized in PyMOL.

Subcellular Localization Using Fluorescence Microscopy

Full-length cDNAs encoding BAM1, -2, -3, and -4 were obtained from the Institut National de la Recherche Agronomique Plant Genomics Research Unit (Versailles, France), the ABRC, or cloned in-house by RT-PCR. For localization in *Arabidopsis* leaf mesophyll protoplasts, the coding sequences were cloned into the binary vector pB7YWG2 by recombinant cloning (Karimi et al., 2005). These constructs produced full-length BAM proteins with YFP fused to their C termini under the transcriptional control of the 35S CaMV promoter. Protoplasts were prepared from wild-type plants according to Fitzpatrick and Keegstra (2001). Transient expression was performed by polyethylene glycol–mediated transfection performed as described by Jin et al. (2001). Fluorescence was viewed with a Leica

TCS SP confocal laser scanning microscope. Fluorophores were excited using a wavelength of 488 nm. The YFP emission signal was collected between 505 and 545 nm. Chlorophyll autofluorescence was collected between 617 and 663 nm.

For localization studies in *Arabidopsis* cultured cells, the coding sequences for BAM2, -3, and -4 were cloned in vector pGWB5 (Karimi et al., 2005), producing full-length BAM proteins with GFP fused to their C termini under the transcriptional control of the 35S CaMV promoter. Additionally, the full-length BAM3 coding sequence was cloned in the vector RFP2-GTWB6 (Karimi et al., 2005), resulting in RFP fused to its C terminus. For a chloroplast marker, the gene encoding the pea (*Pisum sativum*) Rubisco small subunit fused at its C terminus to RFP was cloned in a pGEM-T vector (Promega) containing an expression cassette driven by the 35S CaMV promoter (Chew et al., 2003). The plasmids were precipitated onto gold particles using 2.5 M $CaCl_2$ and 100 mM spermidine. Biolistic bombardment with 0.5 mg of particles into suspension culture cells was performed under vacuum using helium at a pressure of 1400 kPa. Cells were incubated for 16 h on solid medium and analyzed by fluorescence microscopy using an Olympus BX3 microscope with CellR imaging software.

Expression of Recombinant Proteins in *Escherichia coli*

Sequences encoding the four BAM proteins were cloned into the *E. coli* expression vector pGEX-4T-1 for BAM1 and pGEX-2T for the others (Amersham Biosciences). In each case, the N-terminal sequence including the predicted transit peptide was removed (41, 55, and 85 amino acid residues for BAM1, BAM2, and BAM3, respectively). In the case of BAM4, four different recombinant proteins lacking 0, 45, 85, and 90 amino acids were expressed and analyzed, each yielding the same results. The resultant constructs encoded the respective BAM with GST fused to its C terminus. Proteins expressed in the *E. coli* strains BL21 or BL21CodonPlus (DE3)-RIL (Stratagene) were extracted and affinity-purified to near homogeneity using Glutathione–Sepharose 4B according to the manufacturer's protocol (Amersham Biosciences).

Knockout Mutant Analysis

Insertion sites of the T-DNAs of lines from the Salk Institute were characterized using the T-DNA–specific primer 5′-GCGTGGACCGCTTGCTGCAACT-3′ in combination with the appropriate gene-specific primers, as follows: *BAM1*-specific primers, 5′-AGAACGTATAGAGAAGGAGGGATTG-3′ and 5′-CCGTCTCTGAACCTTGTGTTGTAGTA-3′; *BAM2*-specific primers, 5′-GGCGATTAGGTTGAATCATAGTGTA-3′ and 5′-CAGATAGGACAGCACAGCAGA-3′; *BAM4*-specific primers, 5′-GATTGGAGACGTCAATAAGGACAT-3′ and 5′-TCTGCACTCATCTGTCTAATGAAA-3′. The mutation in *bam3* was identified by amplifying a 650-bp fragment with the *BAM3*-specific primers 5′-GAACAAGTGGACCTCATGATG-3′ and 5′-TGAGAGTCTCCTCCCATGAC-3′. The wild-type amplicon is susceptible to digestion with *Bsr*I, whereas the *bam3* fragment is not. RT-PCR on cDNA derived from the wild type and mutants was conducted with the following primer combinations; *BAM1*; 5′-AGAACGTATAGAGAAGGAGGGATTG-3′ and 5′-CGTCTCTGAACCTTGTGTTGTAGTA-3′; *BAM2*, 5′-GGCGATTAGGTTGAATCATAGTGTAA-3′ and 5′-TGGTCTCTTGTGTCCCTGGAGCCAAACCAA-3′; *BAM3*, 5′-GAGCTTATACAGATGGTTCAAAAGC-3′ and 5′-AATCTGACCTATTTGTTGCTACCAC-3′; *BAM4*, 5′-GATGCTCGAGAGAAATCACGATCG-3′ and 5′-TCTGCACTCATCTGTCTAATGAAAG-3′; Actin, 5′-ATTCAGATGCCCAGAAGTCTTGTT-3′ and 5′-GAAACATTTTCTGTGAACGATTCCT-3′. T-DNA insertion mutants from the GABI_KAT collection were characterized using the T-DNA–specific primer 5′-CCCATTTGGACGTGAATGTAGACAC-3′ in combination with the appropriate gene-specific primers, as follows: *BAM1*-specific primers, 5′-TTCGTCAAGGATATTCCTTTTTATG-3′ and 5′-AATCGGAAGTTTTGTGTGACG-3′; *BAM2*-specific primers, 5′-AACCAATGATTCTTGGATCCC-3′ and 5′-AACACGTTGCTTGTCAATTCC-3′.

Lines carrying multiple mutations were obtained by crossing and selecting homozygous plants of the required genotypes from the segregating F2 populations using PCR- and cleaved-amplified polymorphic sequence–based genotyping. To control for the presence of unlinked secondary mutations that might affect the mutant phenotypes, we routinely confirmed that the offspring of different isolates of each genotype were phenotypically similar in terms of growth rate, starch content, and maltose content.

Molecular Design of BAM2 and BAM3 Antigens and Immunoblot Analysis

Antiserum specific for the BAM1 protein was a gift from Jychian Chen (Academia Sinica, Taipei, Taiwan) and was generated by immunization of rabbits with the recombinant protein. Antisera specific for BAM2, -3, and -4 were purchased from Sigma Genosys. Rabbits were immunized with isoform-specific peptides (LRAESTEEDRVPID, RLSKEDTTGSDLYV, and RIFSMDAREKSR for BAM2, -3, and -4, respectively) conjugated to keyhole limpet hemacyanin. Antisera from rabbits immunized with the BAM4-specific peptide did not recognize the recombinant BAM4 protein and therefore could not be used. Anti-BAM3 antibodies were purified via immunoaffinity purification using a column containing the covalently bound peptide antigen. Blots were developed using Sigma-Fast (Sigma-Aldrich) reagents.

Complementation of the *bam4* Mutation

For complementation of the *bam4* mutant, a 2000-bp DNA fragment upstream of the *BAM4* start codon (harboring the promoter), the full-length BAM4 coding sequence, and the StrepII tag (IBA) were amplified separately by PCR with primers containing the Gateway Technology (Invitrogen) *attb* recognition sequences and cloned in appropriate pDONR vectors. The three fragments were combined simultaneously in the multisite cloning vector pH7m34GW (Karimi et al., 2005), resulting in a construct encoding BAM4 with the StrepII tag fused to its C terminus, with expression driven by the *BAM4* promoter. This construct was introduced into the *bam4* mutant by *Agrobacterium tumefaciens*–mediated transformation (Clough and Bent, 1998). Transformed plants were selected on Murashige and Skoog plates containing hygromycin. Transformants were analyzed by RT-PCR to confirm expression of the transgene. T2 plants harboring the transgene were analyzed by iodine staining after decolorization in hot 80% (v/v) ethanol.

Detection of Amylases and Amylolytic Activity

Soluble proteins were extracted from leaves by homogenization in extraction medium containing 100 mM Tris, pH 7.0, 10% (v/v) ethanediol, 5 mM DTT, and 1 mM EDTA. Activities of α-amylase and β-amylase were measured using the Ceralpha and Betamyl assay kits from Megazyme, according to Zeeman et al. (1998a). Alternatively, β-amylase was assayed as described by Zeeman et al. (1998b), except that potato (*Solanum tuberosum*) amylopectin (Sigma-Aldrich) was the substrate rather than soluble starch and the maltose released was measured by high performance anion-exchange chromatography (HPAEC) with pulsed amperometric detection (PAD) on a Bio LC apparatus (Dionex). All assays were done in the presence of DTT (5 mM). For α-amylase measurements, assays were done in the presence of 1 mM $CaCl_2$.

Extraction and Measurement of Metabolites

Two sampling strategies were used. Samples (580 mg mean fresh weight) comprising all of the leaves of an individual plant (30 to 35 d old,

depending on the genotype) were harvested into liquid N_2 and extracted in 0.7 M perchloric acid using an all-glass homogenizer exactly as described (Delatte et al., 2005). Alternatively, entire rosettes (100 mg mean fresh weight) of individual plants (21 to 28 d old, depending on the genotype) were frozen in 96-format collection tubes and pulverized while still frozen using a Mixer Mill (Retsch). The frozen powder was extracted in ice-cold 0.7 M perchloric acid for 30 min with intermittent mixing. Subsequent steps were as described (Delatte et al., 2005). Starch in the insoluble fraction was determined by measuring the amount of glucose released by treatment with α-amylase and amyloglucosidase, as described previously (Smith and Zeeman, 2006). Maltose and larger malto-oligosaccharides in the soluble fraction were determined using HPAEC-PAD. Samples of the neutralized soluble fraction (100 μL) were applied to sequential 1.5-mL columns of Dowex 50 W and Dowex 1 (Sigma-Aldrich). The neutral compounds were eluted with 4 mL of water, lyophilized, and redissolved in 100 μL of water. Maltose was separated on a Dionex PA-100 column according to the following conditions: eluent A, 100 mM NaOH; eluent B, 100 mM NaOH and 50 mM sodium acetate; eluent C, 150 mM NaOH and 500 mM sodium acetate. The gradient was as follows: 0 to 5 min, 50% A and 50% B; 5 to 25 min, a concave gradient to 50% A, 10% B, and 40% C (malto-oligosaccharide elution); 25 to 32 min, step to 10% B and 90% C (column wash step); 32 to 36 min, step to 50% A and 50% B (column reequilibration). Peaks were identified by coelution with known malto-oligosaccharide standards. Peak areas were determined using Chromeleon software. Susceptibility of the detected compounds to digestion by α-glucosidase was confirmed, and recovery experiments, in which physiological amounts of maltose were added to the soluble fraction prior to the Dowex column step, were performed routinely, yielding a mean recovery of 94 ± 1.2% ($n = 94$).

Accession Numbers

Arabidopsis Genome Initiative gene codes for the *Arabidopsis BAM* genes used and discussed in this study are provided in Supplemental Table 1 online. GenBank accession numbers for the genes used to create the phylogenetic tree in Figure 1A are provided in Supplemental Table 2 online, and protein sequences are provided as Supplemental Data Sets 1 and 2 online. Line identifiers for mutants obtained from the SALK, GABI_KAT, and TILLING collections are given in Figure 1.

Supplemental Data

The following materials are available in the online version of this article.

Supplemental Figure 1. Localization of the BAM8-YFP Fusion Protein.

Supplemental Figure 2. Analysis of Lines with T-DNA Insertions in *BAM1* and *BAM2* Genes.

Supplemental Figure 3. β-Amylase Activity in the *ram1* Mutant.

Supplemental Figure 4. Complementation of the *bam4* Mutant Phenotype.

Supplemental Figure 5. α-Amylase Activity in the Wild Type and *bam* Mutants.

Supplemental Table 1. Arabidopsis Genome Initiative Gene Codes and Alternative Nomenclatures for the *Arabidopsis* β-Amylase Gene Family.

Supplemental Table 2. GenBank Accession Numbers of Protein Sequences Used to Create the Phylogenetic Tree in Figure 1A.

Supplemental Data Set 1. Aligned β-Amylase Protein Sequences Used for the Construction of the Phylogenetic Tree Given in Figure 1A.

Supplemental Data Set 2. Alignment of *Arabidopsis* β-Amylase Protein Sequences with the Soybean β-Amylase Gm BMY1, as Shown in Figure 4.

Supplemental References.

ACKNOWLEDGMENTS

We thank the Salk Institute Genomic Analysis Laboratory, the GABI-Kat project, the *Arabidopsis* TILLING Program, and the European *Arabidopsis* Stock Centre for providing the *Arabidopsis* mutants. We thank Hannah Dunstan for assistance with plant growth, Susan Gibson for seeds of the *ram1* mutant, and Jychian Chen for providing the BAM1 and AMY3 antibodies. This work was funded by ETH Zurich, the Roche Research Foundation, the National Centre for Competence in Research–Plant Survival (the Swiss National Science Foundation), the Biotechnology and Biological Sciences Research Council of the United Kingdom (Grant 15/D20100), the Australian Research Council (Grants DP0666434, FF0457721, and CE0561495), and the Government of Australia, Centres of Excellence scheme.

Received October 26, 2007; revised February 21, 2008; accepted March 20, 2008; published April 4, 2008.

REFERENCES

Anderson, S., and Smith, S.M. (1986). Synthesis of the small subunit of ribulose bisphosphate carboxylase from genes cloned into plasmids containing the SP6 promoter. Biochem. J. **240:** 709–715.

Asatsuma, S., Sawada, C., Itoh, K., Okito, M., Kitajima, A., and Mitsui, T. (2005). Involvement of α-amylase I-1 in starch degradation in rice chloroplasts. Plant Cell Physiol. **46:** 858–869.

Baker, N.A., Sept, D., Joseph, S., Holst, M.J., and McCammon, J.A. (2001). Electrostatics of nanosystems: Application to microtubules and the ribosome. Proc. Natl. Acad. Sci. USA **98:** 10037–10041.

Baunsgaard, L., Lütken, H., Mikkelsen, R., Glaring, M.A., Pham, T.T., and Blennow, A. (2005). A novel isoform of glucan, water dikinase phosphorylates pre-phosphorylated α-glucans and is involved in starch degradation in *Arabidopsis.* Plant J. **41:** 595–605.

Buchanan, B.B., and Balmer, Y. (2005). Redox regulation: A broadening horizon. Annu. Rev. Plant Biol. **56:** 187–220.

Cheong, C.G., Eom, S.H., Chang, C.-S., Shin, D.H., Song, H.K., Min, K.-S., Moon, J.H., Kim, K.K., Hwang, K.Y., and Suh, S.W. (1995). Crystallization, molecular replacement solution, and refinement of tetrameric β-amylase from sweet-potato. Proteins Struct. Funct. Genet. **21:** 105–117.

Chew, O., Rudhe, C., Glaser, E., and Whelan, J. (2003). Characterization of the targeting signal of dual-targeted pea glutathione reductase. Plant Mol. Biol. **53:** 341–356.

Chia, T., Thorneycroft, D., Chapple, A., Messerli, G., Chen, J., Zeeman, S.C., Smith, S.M., and Smith, A.M. (2004). A cytosolic glucosyltransferase is required for conversion of starch to sucrose in *Arabidopsis* leaves at night. Plant J. **37:** 853–863.

Clamp, M., Cuff, J., Searle, S.M., and Barton, G.J. (2004). The Jalview Java alignment editor. Bioinformatics **20:** 426–427.

Clough, S.J., and Bent, A.F. (1998). Floral dip: A simplified method for *Agrobacterium*-mediated transformation of *Arabidopsis thaliana.* Plant J. **16:** 735–743.

Collaborative Computational Project, Number 4 (1994). The CCP4 suite: Programs for protein crystallography. Acta Crystallogr. D Biol. Crystallogr. **50:** 760–763.

Critchley, J.H., Zeeman, S.C., Takaha, T., Smith, A.M., and Smith, S.M. (2001). A critical role for disproportionating enzyme in starch breakdown is revealed by a knock-out mutation in *Arabidopsis.* Plant J. **26:** 89–100.

DeLano, W.L. (2002). The PyMOL Molecular Graphics System. (Palo Alto, CA: DeLano Scientific).

Delatte, T., Trevisan, M., Parker, M.L., and Zeeman, S.C. (2005). *Arabidopsis* mutants *Atisa1* and *Atisa2* have identical phenotypes and lack the same multimeric isoamylase, which influences the branch point distribution of amylopectin during starch synthesis. Plant J. **41:** 815–830.

Delatte, T., Umhang, M., Trevisan, M., Eicke, S., Thorneycroft, D., Smith, S.M., and Zeeman, S.C. (2006). Evidence for distinct mechanisms of starch granule breakdown in plants. J. Biol. Chem. **281:** 12050–12059.

Edgar, R.C. (2004). MUSCLE: Multiple sequence alignment with high accuracy and high throughput. Nucleic Acids Res. **32:** 1792–1797.

Edner, C., Li, J., Albrecht, T., Mahlow, S., Hejazi, M., Hussain, H., Kaplan, F., Guy, C., Smith, S.M., Steup, M., and Ritte, G. (2007). Glucan, water dikinase activity stimulates breakdown of starch granules by plastidic β-amylases. Plant Physiol. **145:** 17–28.

Emanuelsson, O., Nielsen, H., Brunak, S., and Von Heijne, G. (2000). Predicting subcellular localization of proteins based on their N-terminal amino acid sequence. J. Mol. Biol. **300:** 1005–1016.

Emanuelsson, O., Nielsen, H., and Von Heijne, G. (1999). ChloroP, a neural network-based method for predicting chloroplast transit peptides and their cleavage sites. Protein Sci. **8:** 978–984.

Fitzpatrick, L.M., and Keegstra, K. (2001). A method for isolating a high yield of *Arabidopsis* chloroplasts capable of efficient import of precursor proteins. Plant J. **27:** 59–65.

Gonnet, G.H., Hallett, M.T., Korostensky, C., and Bernardin, L. (2000). Darwin v. 2.0: An interpreted computer language for the biosciences. Bioinformatics **16:** 101–103.

Guindon, S., and Gascuel, O. (2003). A simple, fast, and accurate algorithm to estimate large phylogenies by maximum likelihood. Syst. Biol. **52:** 696–704.

Hussain, H., Mant, A., Seale, R., Zeeman, S.C., Hinchliffe, E., Edwards, A., Hylton, C., Bornemann, S., Smith, A.M., Martin, C., and Bustos, R. (2003). Three isoforms of isoamylase contribute different catalytic properties for the debranching of potato glucans. Plant Cell **15:** 133–149.

Jin, B.J., Kim, Y.A., Kim, S.J., Lee, S.H., Kim, D.H., Cheong, G.W., and Hwang, I. (2001). A new dynamin-like protein, ADL6, is involved in trafficking from the *trans*-Golgi network to the central vacuole in *Arabidopsis.* Plant Cell **13:** 1511–1526.

Jones, D.T., Taylor, W.R., and Thornton, J.M. (1992). The rapid generation of mutation data matrices from protein sequences. Comput. Appl. Biosci. **8:** 275–282.

Kang, Y.N., Adachi, M., Utsumi, S., and Mikami, B. (2004). The roles of Glu186 and Glu380 in the catalytic reaction of soybean β-amylase. J. Mol. Biol. **339:** 1129–1140.

Kang, Y.N., Tanabe, A., Adachi, M., Utsumi, S., and Mikami, B. (2005). Structural analysis of threonine 342 mutants of soybean β-amylase: Role of a conformational change of the inner loop in the catalytic mechanism. Biochemistry **44:** 5106–5116.

Kaplan, F., and Guy, C.L. (2005). RNA interference of *Arabidopsis* β-amylase 8 prevents maltose accumulation upon cold shock and increases sensitivity of PSII photochemical efficiency to freezing stress. Plant J. **44:** 730–743.

Kaplan, F., Sung, D.Y., and Guy, C.L. (2006). Roles of β-amylase and starch breakdown during temperature stress. Physiol. Plant. **126:** 120–128.

Karimi, M., De Meyer, B., and Hilson, P. (2005). Modular cloning and expression of tagged fluorescent protein in plant cells. Trends Plant Sci. **10:** 103–105.

Kolbe, A., Tiessen, A., Schluepmann, H., Paul, M., Ulrich, S., and Geigenberger, P. (2005). Trehalose 6-phosphate regulates starch synthesis via posttranslational redox activation of ADP-glucose pyrophosphorylase. Proc. Natl. Acad. Sci. USA **102:** 11118–11123.

Kötting, O., Pusch, K., Tiessen, A., Geigenberger, P., Steup, M., and Ritte, G. (2005). Identification of a novel enzyme required for starch metabolism in *Arabidopsis* leaves. The phosphoglucan, water dikinase. Plant Physiol. **137:** 242–252.

Laby, R.J., Kim, D., and Gibson, S.I. (2001). The *ram1* mutant of *Arabidopsis* exhibits severely decreased β-amylase activity. Plant Physiol. **127:** 1798–1807.

Lao, N.T., Schoneveld, O., Mould, R.M., Hibberd, J.M., Gray, J.C., and Kavanagh, T.A. (1999). An *Arabidopsis* gene encoding a chloroplast-targeted β-amylase. Plant J. **20:** 519–527.

Letunic, I., and Bork, P. (2007). Interactive Tree Of Life (iTOL): An online tool for phylogenetic tree display and annotation. Bioinformatics **23:** 127–128.

Livingstone, C.D., and Barton, G.J. (1993). Protein sequence alignments: A strategy for the hierarchical analysis of residue conservation. Bioinformatics **9:** 745–756.

Lloyd, J.R., Blennow, A., Burhenne, K., and Kossmann, J. (2004). Repression of a novel isoform of disproportionating enzyme (*St*DPE2) in potato leads to inhibition of starch degradation in leaves but not tubers stored at low temperature. Plant Physiol. **134:** 1347–1354.

Lloyd, J.R., Kossmann, J., and Ritte, G. (2005). Leaf starch degradation comes out of the shadows. Trends Plant Sci. **10:** 130–137.

Lu, Y., and Sharkey, T.D. (2004). The role of amylomaltase in maltose metabolism in the cytosol of photosynthetic cells. Planta **218:** 466–473.

Lu, Y., Steichen, J.M., Weise, S.E., and Sharkey, T.D. (2006). Cellular and organ level localization of maltose in maltose-excess *Arabidopsis* mutants. Planta **224:** 935–943.

Mikami, B., Degano, M., Hehre, E.J., and Sacchettini, J.C. (1994). Crystal-structures of soybean β-amylase reacted with β-maltose and maltal—Active-site components and their apparent roles in catalysis. Biochemistry **33:** 7779–7787.

Mikami, B., Hehre, E.J., Sato, M., Katsube, Y., Hirose, M., Morita, Y., and Sacchettini, J.C. (1993). The 2.0-angstrom resolution structure of soybean β-amylase complexed with α-cyclodextrin. Biochemistry **32:** 6836–6845.

Mikkelsen, R., Mutenda, K.E., Mant, A., Schürmann, P., and Blennow, A. (2005). α-Glucan, water dikinase (GWD): A plastidic enzyme with redox-regulated and coordinated catalytic activity and binding affinity. Proc. Natl. Acad. Sci. USA **102:** 1785–1790.

Millar, A.H., Sweetlove, L.J., Giege, P., and Leaver, C.J. (2001). Analysis of the Arabidopsis mitochondrial proteome. Plant Physiol. **127:** 1711–1727.

Niittylä, T., Messerli, G., Trevisan, M., Chen, J., Smith, A.M., and Zeeman, S.C. (2004). A previously unknown maltose transporter essential for starch degradation in leaves. Science **303:** 87–89.

Rost, S., Frank, C., and Beck, E. (1996). The chloroplast envelope is permeable for maltose but not for maltodextrins. Biochim. Biophys. Acta **1291:** 221–227.

Scheidig, A., Fröhlich, A., Schulze, S., Lloyd, J.R., and Kossmann, J. (2002). Down regulation of a chloroplast-targeted β-amylase leads to a starch-excess phenotype in leaves. Plant J. **30:** 581–591.

Serrato, A.J., Perez-Ruiz, J.M., Spinola, M.C., and Cejudo, F.J. (2004). A novel NADPH thioredoxin reductase, localized in the chloroplast, which deficiency causes hypersensitivity to abiotic stress in *Arabidopsis thaliana.* J. Biol. Chem. **279:** 43821–43827.

Smith, A.M., and Zeeman, S.C. (2006). Quantification of starch in plant tissues. Nat. Protocols **1:** 1342–1345.

Smith, A.M., Zeeman, S.C., and Smith, S.M. (2005). Starch degradation. Annu. Rev. Plant Biol. **56:** 73–98.

Smith, S.M., Fulton, D.C., Chia, T., Thorneycroft, D., Chapple, A., Dunstan, H., Hylton, C., Zeeman, S.C., and Smith, A.M. (2004). Diurnal changes in the transcriptome encoding enzymes of starch metabolism provide evidence for both transcriptional and posttranscriptional regulation of starch metabolism in Arabidopsis leaves. Plant Physiol. **136:** 2687–2699.

Smith-White, B.J., and Preiss, J. (1992). Comparison of proteins of ADP-glucose pyrophosphorylase from diverse sources. J. Mol. Evol. **34:** 449–464.

Sparla, F., Costa, A., Schiavo, F.L., Pupillo, P., and Trost, P. (2006). Redox regulation of a novel plastid-targeted β-amylase of *Arabidopsis thaliana.* Plant Physiol. **141:** 840–850.

Till, B.J., et al. (2003). Large-scale discovery of induced point mutations with high-throughput TILLING. Genome Res. **13:** 524–530.

Utsumi, Y., and Nakamura, Y. (2006). Structural and enzymatic characterization of the isoamylase1 homo-oligomer and the isoamylase1-isoamylase2 hetero-oligomer from rice endosperm. Planta **225:** 75–87.

Villarejo, A., et al. (2005). Evidence for a protein transported through the secretory pathway en route to the higher plant chloroplast. Nat. Cell Biol. **7:** 1224–1231.

Wang, Q., Monroe, J., and Sjolund, R.D. (1995). Identification and characterisation of a phloem-specific β-amylase. Plant Physiol. **109:** 743–750.

Wattebled, F., Dong, Y., Dumez, S., Delvallé, D., Planchot, R., Berbezy, P., Vyas, D., Colonna, P., Chatterjee, M., Ball, S., and D'Hulst, C. (2005). Mutants of Arabidopsis lacking a chloroplastic isoamylase accumulate phytoglycogen and an abnormal form of amylopectin. Plant Physiol. **138:** 184–195.

Weise, S.E., Kim, K.S., Stewart, R.P., and Sharkey, T.D. (2005). β-Maltose is the metabolically active anomer of maltose during transitory starch degradation. Plant Physiol. **137:** 756–761.

Weise, S.E., Schrader, S.M., Kleinbeck, K.R., and Sharkey, T.D. (2006). Carbon balance and circadian regulation of hydrolytic and phosphorolytic breakdown of transitory starch. Plant Physiol. **141:** 879–886.

Weise, S.E., Weber, A.P.M., and Sharkey, T.D. (2004). Maltose is the major form of carbon exported from the chloroplast at night. Planta **218:** 474–482.

Yu, T.-S., et al. (2001). SEX1 is a general regulator of starch degradation in plants and not the chloroplast hexose transporter. Plant Cell **13:** 1907–1918.

Yu, T.-S., et al. (2005). α-Amylase is not required for breakdown of transitory starch in *Arabidopsis* leaves. J. Biol. Chem. **280:** 9773–9779.

Zeeman, S.C., Northrop, F., Smith, A.M., and ap Rees, T. (1998a). A starch-accumulating mutant of *Arabidopsis thaliana* deficient in a chloroplastic starch-hydrolyzing enzyme. Plant J. **15:** 357–365.

Zeeman, S.C., Smith, S.M., and Smith, A.M. (2007). The diurnal metabolism of leaf starch. Biochem. J. **401:** 13–28.

Zeeman, S.C., Umemoto, T., Lue, W.-L., Au-Yeung, P., Martin, C., Smith, A.M., and Chen, J. (1998b). A mutant of *Arabidopsis* lacking a chloroplastic isoamylase accumulates both starch and phytoglycogen. Plant Cell **10:** 1699–1711.